University of Stavanger

Faculty of Science and Technology

MASTER'S THESIS

Study program/Specialization: Petroleum Geosciences Engineering	Spring, 2017 Open
Writer: Annette Grønberg	Annette Grønberg
Faculty supervisor: Wiktor W. Weibull	
Title of thesis: Wave-equation migration velocity analysis of the successive vintages of the Sleipner Field – A detailed prediction of the mechanical effects caused by CO2 injection	
Credits (ECTS): 30	
Keywords: WEMVA Seismic processing Target Image Fitting Sleipner Carbon Capture and Storage	Pages: 69pp Including one appendix Stavanger, 15th of June, 2017

Wave-equation migration velocity analysis of the successive vintages of the Sleipner Field – A detailed prediction of the mechanical effects caused by CO_2 injection

by

Annette Grønberg

MSc Thesis

Presented to the Faculty of Science and Technology

The University of Stavanger

The University of Stavanger

June 2017

Acknowledgements

Thanks and my deepest appreciation are expressed to my supervisor Assoc. Prof. Wiktor W. Weibull, who with his persistence and dedication has been a big inspiration to me. His support, comprehensive advice, and guidance have been essential for this study end-result. The challenges provided for me through this project has allowed me to grow both personally and professionally.

In addition, I extend my gratitude to my fellow students, with this especially Farid Mahmoud and Øystein Storaas, whom has supported me and granted me with kind endless help and generous consultations throughout this study. For this, I am truly grateful.

Abstract

Wave-equation migration velocity analysis of the successive vintages of the Sleipner Field – A detailed prediction of the mechanical effects caused by CO_2 injection

Annette Grønberg, Master in Petroleum Geoscience

The University of Stavanger, 2017

Supervisor: Wiktor W. Weibull

Since September 1996, Statoil and partners have through their carbon capture and storage project at the Sleipner field, located in the central North Sea, injected approximately one million tons carbon dioxide per year into the sand prone reservoir of the Utsira Formation. From previous studies, it is established a significant reduction in both bulk and shear moduli when substituting brine with gas in a reservoir. In addition, multipathing and poor illumination occur as a result of gas saturation indicating that conventional velocity analysis techniques will be insufficient.

This contribution examines and determines velocity changes in intra-reservoir layers by the use of target image fitting based on a wave-equation migration velocity analysis (WEMVA). Image-domain tomographic methods, such as the WEMVA method, exploits the divergence between the inadequate depth-migrated image and a perfectly focused version of the data. Reducing the uncertainty of the velocity model will be advantageous in signal processing of the data and estimations of gas layer thicknesses. As a result, better estimation of the amount of carbon dioxide stored in the reservoir can be made. In addition, it will be possible to make a more reliable prediction of migration pathways in the reservoir.

It is shown that applying a WEMVA based velocity model constraining velocity changes to known accumulations of carbon dioxide has a satisfying effect on the migrated image. In addition, enhanced focusing of the migrated images for additional reflectors indicates a sufficient and adequate velocity model.

Table of Contents

List of Tables

List of Figures

Chapter 1: Introduction

To properly position reflectors in space, the migration process of the dataset demand an accurate velocity model. Thus, determining a velocity model from the dataset is an essential step in seismic imaging. For this purpose, a geological insight of the subsurface properties and structure may contribute to the understanding of wave propagation velocities. However, for the information to be accurate, it must be retrieved from seismic data. Laboratory evaluation indicates a distinct dependency between both P- and S-wave velocity and the properties of the saturation fluid (Gassmann, 1951; Wyllie et al., 1956; King, 1966; Gardner et al., 1974; Elliott & Wiley, 1975). Through these studies, it is established that both bulk and shear moduli are lower for a gas-saturated reservoir rock than for the same framework saturated with oil or brine. Substituting brine with gas affects the seismic image in time creating a push-down effect below the reservoir as a result of reducing velocities. Depth imaging or depth conversion can be used to obtain the true topography of the reflectors beneath the gas. However, the depth conversion requires an accurate velocity model to produce a precise depth migrated image.

Large quantities CO_2 has since 1996 been injected into a saline aquifer of the Utsira Formation at the Sleipner field. Because of the adjustment in the stress field due to changes in pore pressure and rock volume, the injections have a major mechanical impact on the reservoir that may lead to re-activation of existing faults and loss of reservoir and cap rock integrity, causing leakages. In order to monitor the reservoir and predict its development, extensive quantities of data have been gathered from the Sleipner field the last twenty years. Enhanced seismic reflections have revealed multiple intra-reservoir mudstone layers resulting in sub-horizontal traps and distinct flow units inside a developed gas plume in the reservoir. This information provides a remarkable opportunity to study risks and challenges related to subterranean carbon capture and storage projects. One such challenge is how gas saturated layers affect seismic imaging. As multipathing and poor illumination occurs in areas containing gas, conventional velocity analysis techniques is often insufficient by cause of their ray-based operators (Sava et al., 2004). An accurate velocity model is crucial for properly imaging the reflectors under the gas. Therefore, if the velocity changes due to gas injection can be quantified, these can be used to estimate the how the gas is distributed in the reservoir.

Initial studies focus on quantitative estimates of the intra-reservoir layer thicknesses using conventional and generalized or laboratory determined velocity models in order to evaluate the amount of gas present in the reservoir. Therefore, this thesis will determine velocity changes in intra-reservoir layers by the use of a technique called wave-equation migration

velocity analysis (WEMVA). This technique differs from conventional velocity analysis in that it employs full wave-based operators in the migration and velocity estimation. Wave based operators are accurate in presence of strong and sharp variations of the seismic velocities and suffer from less limitations than the classical asymptotic ray-based operators. This will allow us to obtain more accurate velocity models, improving migration of seismic reflectors under the gas layers and, at the same time, ensure the proper positioning of mud layers inside the gas plume. Reducing the uncertainty of the velocity model will be advantageous in signal processing of the data and estimations of gas layer thicknesses. As a result, better estimation of the distribution of the carbon dioxide stored in the reservoir can be made. In addition, it will be possible to make a more reliable prediction of migration pathways in the reservoir.

Commonly, in conventional time-shift velocity analysis, an assumption of linear perturbation relationship is made. However, the velocity changes significantly with the injection of gas violating the assumption. Therefore, a non-linear analysis is necessary for these situations. Using WEMVA, this study will determine velocity changes in the seismic measurements due to CO_2 injection using time-lapse seismic data collected in 1994, 1996 and 2001 at the Sleipner field. Assuming that the depth of the reservoir base, and hence the reservoir thickness, does not differ due to the injection, the method will be based on determining a velocity model that makes the migration of the reflections beneath the upper boundary of the Utsira Formation to match in depth for all vintages. A baseline model will be produced from the pre-injection 1994 survey. The later vintages will then be iteratively adjusted in order to make key interpreted reflectors match in depth.

Strong and sharp lateral variations in velocities, which are expected as a result of the ongoing CO_2 injections, will not be considered as a challenge when using the WEMVA strategy as this method can handle multipathing and wave propagation in areas with complex geology (Yang & Sava, 2010). In addition, unlike conventional travel time tomography, the method is fully automatic and does not require manually picking travel times, reducing the uncertainties in the results. However, key reflectors need to be manually interpreted on all vintages. These will be used in the co-depth procedure. This process can be demanding as the presence of the gas might perturb the reflections beneath the Utsira Formation, making their interpretation difficult. Problems like acoustic blanking and overlapping interbed multiples are to be expected. Therefore, methods for attenuating the interbed multiples and for de-noising of the reflections beneath the Utsira Formation will be employed in the first stages of the project. WEMVA is a non-linear iterative method that requires large amounts of computer resources. To solve for the

subsurface velocity changes we have used the Clusters provided by the high-performance computing network of UNINETT Sigma2 AS, which offers its services without charge for individuals or groups conducting educational research in Norway.

In order to walk you through the analysis conducted, this thesis is comprised of six parts with its content briefly described as following:

Chapter 1 introduces the following study and explains the importance of an accurately performed velocity analysis.

Chapter 2 gives a description of the carbon capture and storage project at the Sleipner facilities. In addition, site characterization of the reservoir and previous applied geophysical methods will be mentioned.

Chapter 3 describes the datasets constructing the basis of this project and the performed processing steps executed on each dataset. Further, the chapter defines the wave-equation migration velocity analysis that is performed on the given datasets.

Chapter 4 present the results from the analysis based on the developed velocity model with different constraints.

Chapter 5 discusses the results of this study, and compare the different migrated images produced by velocity models with different constraints.

Chapter 6 gives a short conclusion based on the result of the work conducted and results produced.

Chapter 2: The Sleipner CO_2 injection operation

Carbon capture and storage (CCS) projects aim to capture superfluous carbon dioxide and transport it to a storage site avoiding its release to the atmosphere. The intent is to reduce global warming and ocean acidification, preventing the environmental impact of CO_2, as well as to lower tax inflicted on the upstream petroleum industry by the Norwegian government (Halland et al., 2013). The producible gas of the Sleipner West contains carbon dioxide in the range of 4-9 percent (Harvey, 2010). Due to market specifications declaring the maximum CO_2 content of 2.5 percent, the carbon dioxide fraction in this part of the field has to be reduced to an acceptable level to be commercial (Halland et al., 2013).

Since September 1996, Statoil and partners have through their Sleipner project, injected approximately one million tons carbon dioxide per year into the sand prone reservoir of the Utsira Formation located in the central North Sea (Fig. 2.1; Halland et al., 2013). Using a deviated well (15/9-A-16), the gas is injected directly from the platform preventing the need of transportation (Fig. 2.1). CO_2 injection into a saline aquifer has a major mechanical impact that may lead to re-activation of existing faults and loss of reservoir and seal rock integrity. Due to changes in pore pressure and rock volume, as a result of the adjustment in the stress field, the injection may cause leakages (Streit & Siggins, 2005). Hence, the injections have been monitored by projects such as CO2STORE and SACS to verify the project safety and to gain international acceptance (Holloway et al., 2004).

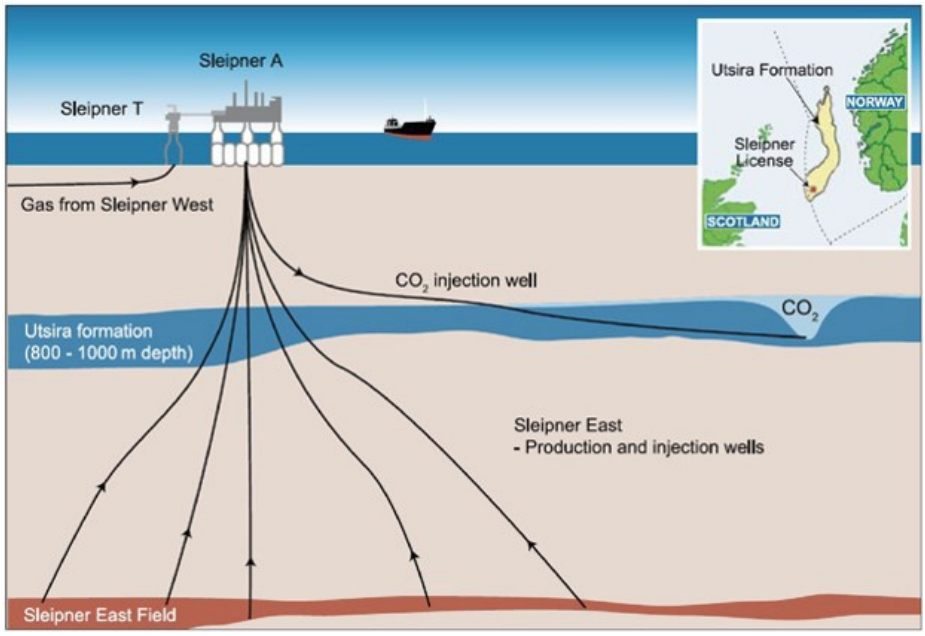

Figure 2.1: Illustration indicating the location of the Utsira Formation and the Sleipner license relative to Norway and Scotland. In addition, the figure demonstrates how CO2 is injected through a deviated well in the Utsira Formation. By IEA GHG, 2008

The multidisciplinary saline aquifer CO_2 storage-project (SACS) was founded in cooperation between a group of energy companies, scientific institutes and environmental authorities in several countries. When the project ended in 2002, parts of the project activities were continued by the EU-cofounded CO2STORE-project. Both projects intend to monitor the carbon dioxide injections in the geological reservoir of Utsira Formation to provide knowledge about the proposed subsurface storage opportunity. Additionally, the project is developed to provide information to assist in developing new opportunities for CO_2 storage, which in its turn may reduce the amount of greenhouse gasses released into the atmosphere.

2.1 Geological setting

As a result of Greenland separating from Norway after the Caledonian Orogeny, and due to failed continental rifting between the Scandinavian and British landmasses during Permian to Mesozoic time, the North Sea basin arose as an epicontinental basin (Gregersen et al., 1997). The Lower Paleozoic crystalline and metamorphic basement rocks underlying the North Sea basin was formed by cause of the closure of the Lapetus Ocean and the Tornquist Sea during the Caledonian Orogeny (Gregersen et al., 1997). Because the basement was established before the formation of oceanic crust, the basin is still located on continental crust (Færseth, 1996; Evans et al., 2003).

The dominant structures of the North Sea were developed during middle Jurassic to the early Cretaceous time when Viking Graben was formed. NW-SE rifting created a graben architecture with an NE-SW direction in the northern part of the North Sea (Fig. 2.2; Færseth, 1996). Major tectonic activities developed several rotated fault blocks and steeply angled faults, as well as horst and graben structures, which led to a basin dominated by post-rifts and regional subsidence (Evans, 2003).

Four main onlap-defined, tectonosequences, corresponding to Paleogene, Eocene, Oligocene, and Miocene, were suggested by Galloway et al. (1993) to be the main depositional episodes of the northern North Sea. Due to a thermal uplift of basin margins during Cenozoic eastward dipping fault blocks was developed. This resulted in several submarine fans, displayed as a deltaic system, which provided basin infill and supplying sandy and silty sediments, originating from the Shetland Platform, located west of Viking Graben, to the basin (Fig. 2.2; Galloway et al., 1993).

Late Oligocene deposits are characterized by a lateral change with of interpenetrating wedges of silt and clays of the Hordaland Group and sand sedimentation of the Skade Formation, indicating a eustatic sea-level fall (Fig. 2.2; Isaksen & Tonstad, 1989; Gregersen et al., 1997). Further, it is suggested that the argillaceous Nordland Group was deposited during Early-Middle Miocene, an epoch that was controlled by low accumulation, lack of tectonic uplift, and a shift in compressive intraplate stress (Fig. 2.2; Rundberg, 1991; Galloway et al., 1993; Gregersen et al., 1997). As a consequence of increasing geostrophic currents and glacial-eustatic sea-level fall followed by a mid-Miocene crustal uplift, deposition of the Upper Miocene to Lower Pliocene Utsira Formation was provided mainly from the Scandinavian mainland (Fig. 2.2; Rundberg, 1991; Ghazi, 1992; Galloway et al., 1993). Glacial erosion of the western coast of the Norwegian mainland then resulted in thick Quaternary sequences in during late Pliocene and Quaternary (Head et al., 2004).

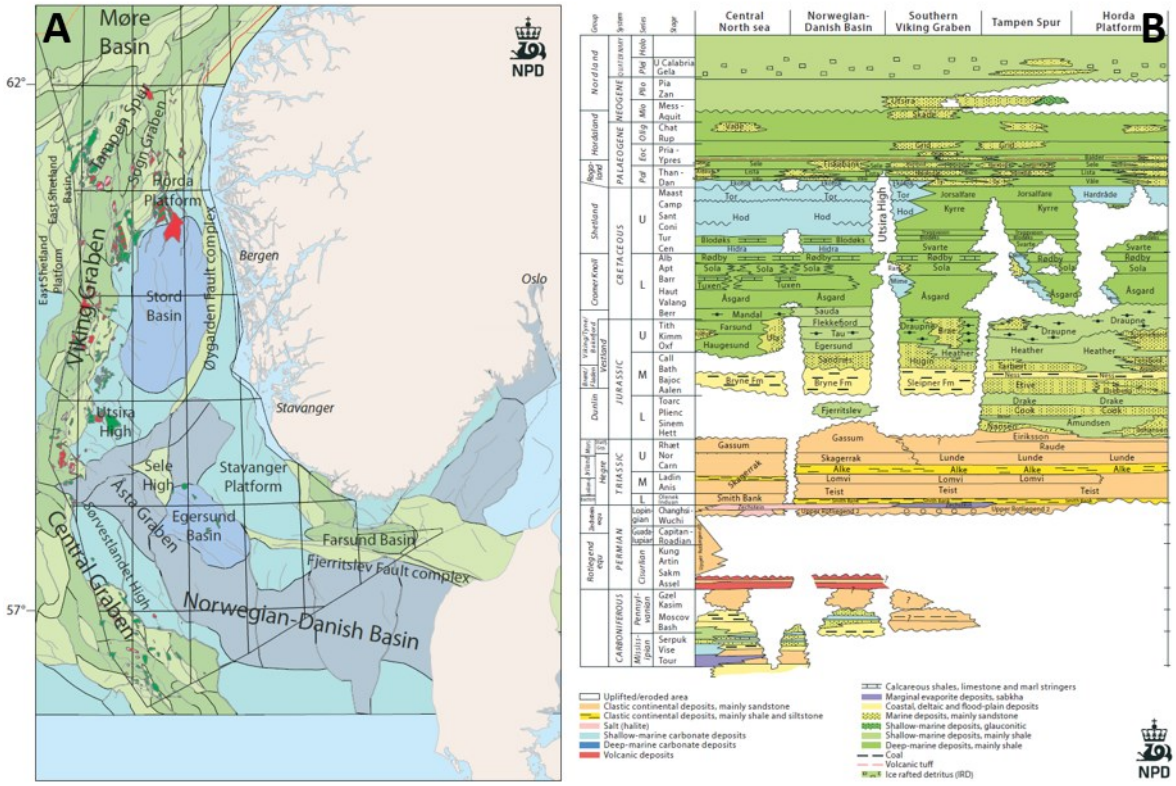

Figure 2.2: A) Main geological structures of the North Sea displaying Viking Graben towards the west and Central Graben towards the southwest. B) Lithostratigraphic chart of main formations present in the North Sea. From Halland et al. (2012).

2.2 The Utsira storage formation

Amongst several alternatives to reduce the release of extracted CO_2 from natural gas into the atmosphere, subsurface storage in the Utsira Formation was chosen. Opportunities such as enhanced oil recovery (EOR) and injection in other formations like Heimdal Formation and Skagerrak Formation, both sites located in the Sleipner East field, was rejected due to its

uncertainties (Korbøl & Kaddour, 1995; Chadwick et al., 2008). As EOR using CO_2 was considered to be unpredictable, while the alternative formations were located close to producible reservoirs and would possibly generate a threat to the production, injection in the Utsira Formation was considered the most reliable alternative (Chadwick et al., 2008).

2.2.1 Extent and geology

Utsira and Skade formations are suggested to form a saline aquifer system located in the Norwegian sector of the North Sea (Halland et al., 2011). However, for the injections in the Sleipner field, the particularly porous (30-40 %), very permeable (1-3 Darcy) and, weakly consolidated marine sandstones of the Middle Miocene to Lower Pliocene Utsira Formation serve as the reservoir rock (Chadwick et al., 2004a; Zweigel et al., 2004). With the main source located to the west, the complex architecture involving elongated sand bodies that extend ~450 km from north to south and ~90 km from east to west (Fig. 2.3; Halland et al., 2011). A thickness map constructed by Torp and Gale (2004) indicates a variable thickness ranging from ~25 m to ~300 m (Fig. 2.3). In addition, with a smooth variation in depth, the Formation is located ~500 m below sea level in the northwestern part of deposition and more than 1500 m below sea level in the northern part (Fig. 2.3; Torp & Gale, 2004).

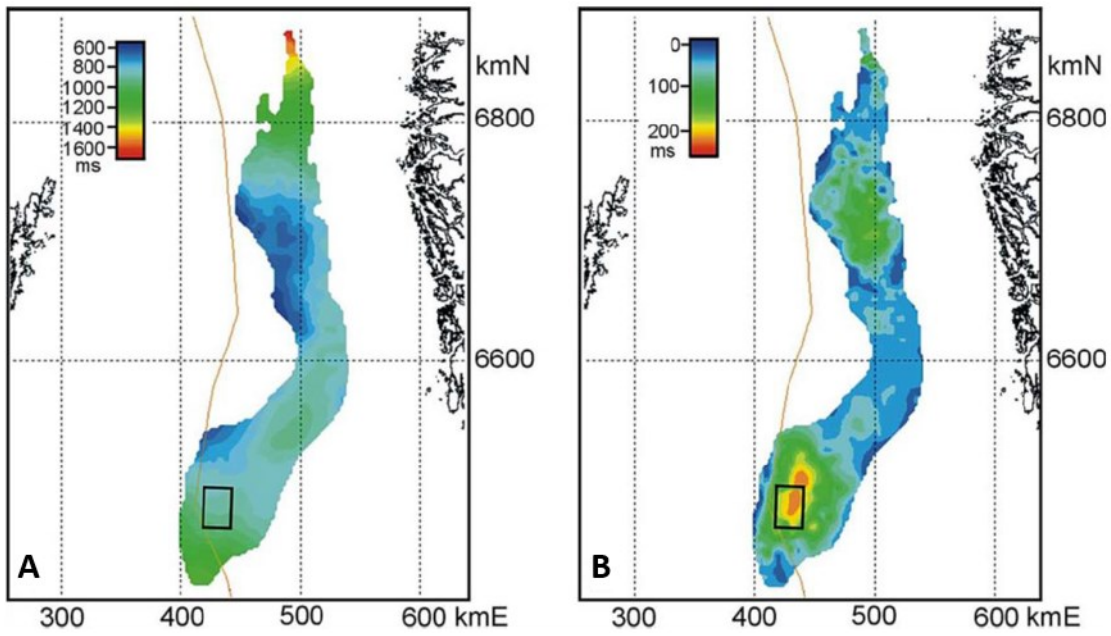

Figure 2.3: The interpreted extent of the Utsira Formation. The black box illustrates the Sleipner license. A) Depth estimation of the upper boundary of Utsira Formation. B) The estimated thickness of the Utsira Formation is calculated from interpreted top and bot

While the northern part of the Utsira Formation, close to Tampen Spur, is consisting of thin beds of glauconitic sands, the southern part is deposited in large mounded sand systems. With an average depth of 800-1100 meters, a thickness of about 200-300 meters and a coverage

of 26'000 km2, the Formation is considered to potentially store gigatons (Gt) of CO_2 in the future (Halland et al., 2011). Due to the Utsira Formation not serving as a previous hydrocarbon reservoir, studies prior to the injection was relatively scarce. Therefore, to avoid breakage of the cap rock, information pre-injection was gained through wire-line logging, 2D seismic data lines and information from drilled wells penetrating the Formation several kilometers away from the injection site (Bickle et al., 2007).

Assuming that the Utsira Formation is a homogenous sand package, the injected gas would be expected to migrate towards and accumulate at the shallowest part of the reservoir. Through monitoring the reservoir, it is found that this is not the case (Chadwick et al., 2004a; Zweigel et al., 2004; Furre & Eiken, 2014). Accumulation of carbon dioxide appears to take place at several locations vertically between the injection point and the shallowest point of the capping structure (Fig. 2.4). Through relatively small spikes in well logs 9-12 thin (<1 meter) impermeable shale and mud stringers have been interpreted interbedded in the formation, creating several flow units, all used for storage of CO_2 (Fig. 2.4; Chadwick et al., 2004a; Furre & Eiken, 2014). One larger spike is observed towards the top reservoir indicating a thicker (6-7 m), more continuous shale layer (Zweigel et al., 2004). In contrast to the thinner shale stringers, the top shale layer has been correlated between several wells, indicating a growth in the upper sand package in the east-west direction (Valberg, 2014). Such a variating, even if small, dip in the Utsira upper surface may have a significant impact on the migration route of the injected carbon dioxide.

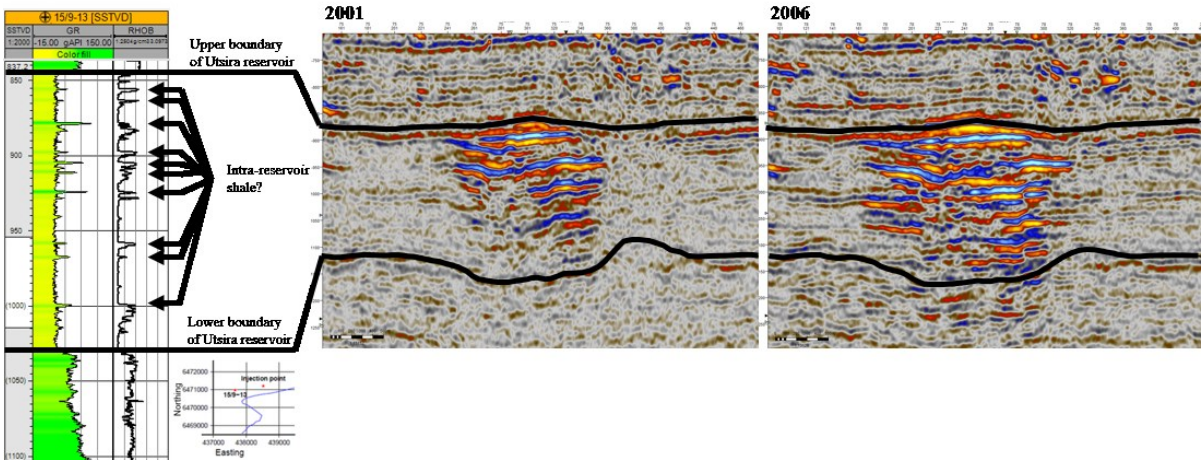

Figure 2.4: Gamma-ray and density logs for well 15/9-13 indicating several intra-reservoir shale and/or mudstone layers. Unmigrated seismic images from surveys conducted in 2001 and 2006 demonstrates how CO2 is accumulating beneath the shale layers instead of migrating directly to the shallowest part of the reservoir.

The upper boundary of the Utsira Formation has indications of local depressions. This, combined with mud diapirs and mud volcanoes at the Utsira base, is considered the reason for the varying thickness and domal structures of the Utsira reservoir (Fig. 2.3; Zweigel et al., 2004). Aside from at the margins of diapirs, the Formation has no indication of internal faulting (Valberg, 2014).

2.2.2 Direct over- and underburden sealing units of the Utsira reservoir

Prior to the injection, a thorough assessment of the storage capacity of the overburden cap rock of was conducted. Particular, an enhanced confidence in the sealing capacity was critical in order to be certain that no, or at least minimal, leakage would occur as carbon dioxide was injected to the subsurface. An analysis of cuttings from core samples was tested to determine the capacity of the overburden sediments. Results indicated a remarkable sealing capacity of the capping rock, with a dimension able of holding a super-critical CO_2-column of several hundred meters (Chadwick et al., 2004a; Harrington et al., 2009; Chadwick et al., 2012).

The overall sealing unit is considered to be the Nordland shales deposited directly above the Utsira Formation. It has a thickness ranging from 200 to 300 meters and a varying lithology of shale in the axial to silt and sandstone in the marginal basin. The overburden is divided into three main units where the deepest unit is considered the primary capping rock for the reservoir (Gregersen et al., 1997; Chadwick et al., 2004a). The unit is strictly restricted to the basin and has a thickness of 50-100 m (Chadwick et al., 2008). The overlying unit consists of a Pliocene prograding wedge of approximately 100 m thickness, while the Quaternary glaciomarine clays are considered as the uppermost sealing unit for the reservoir (Gregersen et al., 1997).

The underlying is comprised of gas charged, muddy and soft sediments of the Hordaland Group, rapidly deposited during Oligocene to Lower Miocene (Gregersen et al., 1997; Zweigel et al., 2004). At the boundary between the Hordaland Group and the overlying Utsira Formation, mud volcanoes and diapirs with faulting at the margins are found (Zweigel et al., 2004; Chadwick et al., 2008). Therefore, it is important to consider that, if later reactivated, these faults may act as a threat to the sealing capacity in later periods (Valberg, 2014).

2.2.3 Injection rate and storage capacity

Carbon dioxide is injected directly below a dome structure with a diameter of about 1200 meters in the Utsira Formation (Zweigel et al., 2004). With channel bodies linking the dome to similar features within the formation, the spill point of the reservoir is found to be approximately 12 meters below the injection point (Zweigel et al., 2004). The maximum storage capacity of the Utsira Formation, determined by its extent and average reservoir properties, is calculated to be

~6 x 10^{11} m^3 (Chadwick et al., 2004a; Pham et al., 2013; Lothe et al., 2014). However, a more reasonable estimate would require the total pore volume of the reservoir. Considering the low relief of the Utsira reservoir the aforementioned value cannot be utilized (Halland et al., 2011). Nonetheless, capacity evaluation ought to consider physical storage capacity within pores in reservoirs close to the structural heights in the area of predicted migration distances. Combining the average porosity of the Formation with the predicted migration distances in the reservoir in the calculations, the expected storage capacity is approximately 5.26 x 10^{11} m^3 (Pham et al., 2013; Lothe et al., 2014). Due to the use of average properties, in addition to not being able to predict the effective pore volume, this result is not accurate enough. However, as an estimate the storage capacity calculations is valid.

2.3 Previous applied geophysical evaluation methods

Being the first large-scale offshore CCS project using a geological formation as storage, the Sleipner project has had to master the challenges that appear with no prior experience to take advantage of. Therefore, to monitor the injected carbon dioxide in the Utsira Formation accurately several geophysical methods has been carried out. Geophysical monitoring tools were implemented rather than direct measurements from observations well to avoid the risk of puncturing the cap rock (Eiken et al., 2000). Among others, 3D seismic and gravity surveying, reservoir simulation tools, laboratory experiments, and reservoir simulations have been carried out in order to achieve a satisfying overview of the subsurface carbon dioxide accumulation.

The CO2STORE and SACS projects have had a major success demonstrating the monitoring possibilities due to conventional time-lapse surveys. A seismic survey was conducted in 1994 - two years before injection. Following, time-lapse surveys was gathered in 1999, 2001, 2002, 2004, 2006, 2008, 2010 and 2013. Combining the 3D datasets to a 4D cube produces an image of the plume development with time related to the changing gas saturation in the reservoir.

To improve the estimation of reserves and for decision-making purposes reservoir simulations have been made (Holloway et al., 2004; Andrew et al., 2015).By combining geological and reservoir models, a digital imitation of the subsurface storage facility has been constructed to design a numerical equivalent three-dimensional geological map and improve understanding of the reservoir (Fig. 2.5; Arts et al., 2004a). The resulting reservoir simulations confirm the prediction of a long life storing possibility (Torp & Gale, 2004). However, accurately imitating the drainage displacement of CO_2 replacing brine at a large time scale is challenging (Andrew et al., 2015). Therefore, multiple geophysical methods have been applied

to the Sleipner field vintages in order to estimate thicknesses of gas accumulations and local velocity changes in the seismic data. This information has had a large impact on the certainty of volume calculations and prediction of migration routes and has aided to establish the safety of underground storage of carbon dioxide.

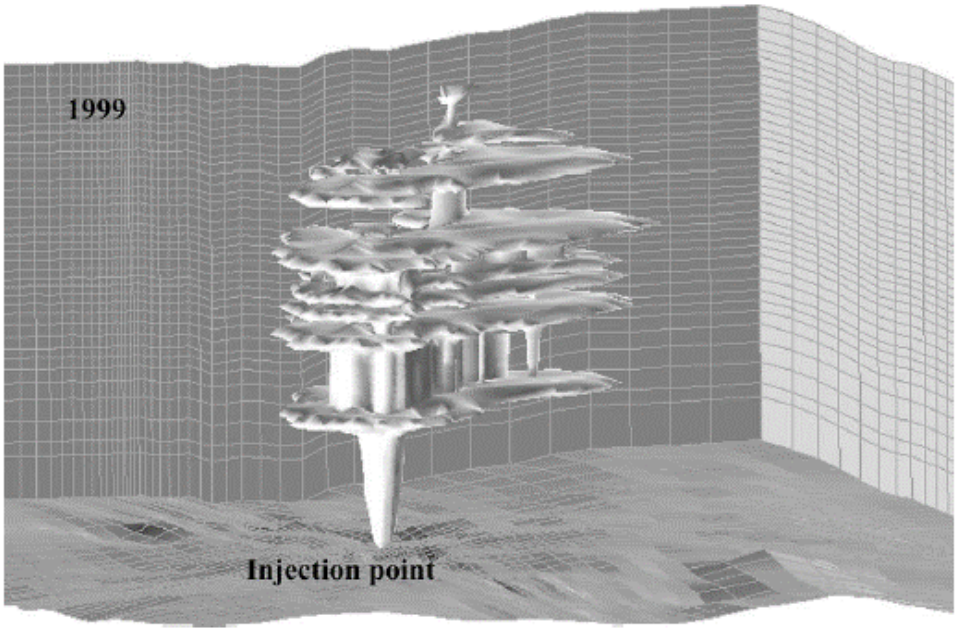

Figure 2.5: Digital reservoir simulation of the monitoring seismic survey conducted in 1999 illustrating the reservoir framework and the predicted migration routes creating communication between different layer accumulations of carbon dioxide. From Arts et al. (2004a).

2.3.1 Gassmann's equation for fluid substitution

As a response to the gas injections in the reservoir, seismic amplitudes indicate a significant push-down effect, both increasing noise level and decreasing the seismic velocities of horizons below the gas cloud. Accordingly, petro-acoustic and thermodynamic methods have been applied in order to relate bulk and shear moduli to the reservoir properties, and further evaluate the influence of fluid substitution (Art et al., 2004b; Andrew et al., 2015).

Relating the bulk modulus of a rock to its pore, frame and fluid properties, the Gassmann's model (Gassmann, 1951) is often preferred in order to analyze the effect of fluid substitution in a reservoir. Assuming known properties of the host rock, the original fluid in place and the injected fluid, Gassmann calculations has been implemented on data acquired at the Sleipner field (Art et al., 2004a). The results suggest a relatively constant P-wave velocity

within a CO_2 saturation interval between 20 to 100 %, directly compared to calculations for the host rock with 100 % water saturation (Fig. 2.6; Arts et al., 2004a; Gutierrez et al., 2012).

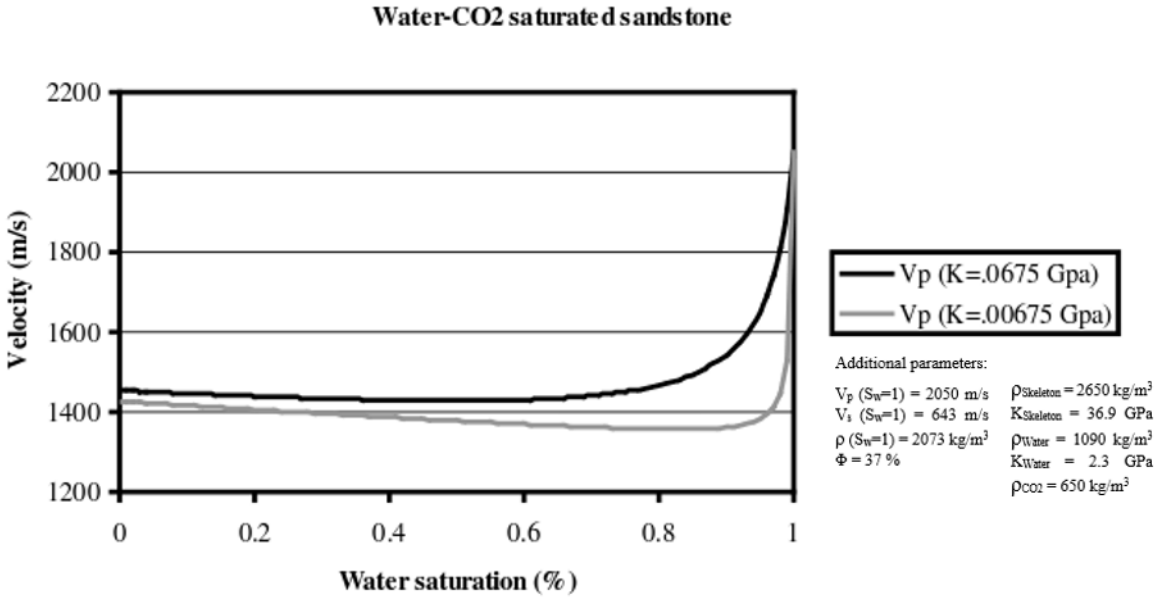

Figure 2.6: P-wave velocity derived from the Utsira Formation as a function of water saturation (1-CO2) using Gassmann's model (Arts et al. 2004a).

The accuracy of Gassmann calculations depends on the quality of the well logs from which essential information of formation property and initial fluid properties estimation is made (Kumar, 2006). As a result of the low relief of the Utsira reservoir, an accurate velocity estimation is crucial for the time-depth conversion as small errors may have a large effect on the estimation of the trapping mechanism and migration routes (Cameron et al., 2008). Although the resulting relationship between P-wave velocity and gas in place may be reasonable, it is important to stress that the results of the Gassmann's model can isolate only be used as a priori quantitative knowledge, as the model uncertainty has an essential effect on the variance of the P-wave velocity of a rock saturated with fluid (Artola & Alvarado, 2006).

2.3.2 Quantitative seismic analysis using seismic amplitudes and time-shift analysis

The assessment of both thickness and velocities of the sub-horizontal layers in the gas plume has been conducted using multiple techniques. Comparing the synthetic seismogram to the original seismic signal, a correlation is to be found for top and bottom boundaries for the Utsira Formation (Delépine et al., 2011). As a result of interference between intra-reservoir layers and the underlying carbon dioxide, it is found that the thickness of CO_2 layers may be estimated directly from the reflection amplitudes (Fig. 2.7; Chadwick et al., 2004b; Chadwick et al., 2005; Bickle et al., 2007; Chadwick et al., 2008; Arts et al., 2009; Delépine et al., 2011). Due to the narrow thickness of intra-reservoir shale units, the correlation coefficient inside the reservoir is

not that adequate (Chadwick et al., 2005). The results give an indication of thin-layer thicknesses but provide no information on velocity changes due to carbon dioxide. In addition, the resulting non-linear relationship between amplitude and thickness tends to indicate diminishing results above and around the tuning thickness (Chadwick et al., 2009; Williams & Chadwick, 2012).

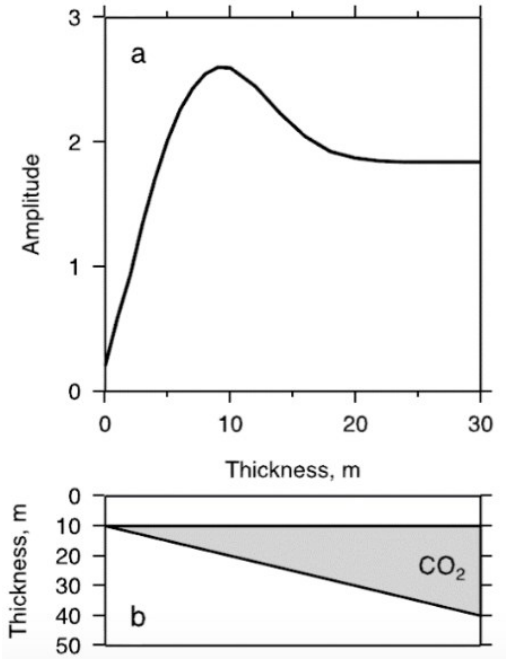

Figure 2. 7: Illustration of amplitude variations as a function of accumulated gas beneath the reflection. (Boait et al., 2012).

Attempting to find the amount of gas needed to produce the highest possible amplitude, the trend as amplitude change with injected gas in the Utsira reservoir was studied (Bickle et al., 2007; Boait et al., 2012). The results indicate a very complex study with a high dependency on the actual thickness of the local intra-reservoir sealing units, in addition to the tuning effect of the CO_2. Hence, more research should be done to produce reliable results.

Supplementary, several studies have aimed to estimate layer thicknesses and velocity anomalies by combining seismic amplitudes and time-shift analysis (Art et al., 2004a; Chadwick et al., 2004b; Chadwick et al., 2005; Ghaderi & Landrø, 2009). By concentrating on the visible push-down effect on the base reflector of Utsira formation, an average time-shift for reservoir units was determined (Fig. 2.8). Using time-lapse data from 1999, 2001 and 2002 and exploring a thin CO_2 layer which does not manufacture multiples affecting the Utsira base, the model of Ghaderi & Landrø (2009) indicated a constant layer thickness of 15 meters and a

velocity change of 200 m/s, 400 m/s, and 500 m/s, respectively (Tab. 2.1; Ghaderi & Landrø, 2009).

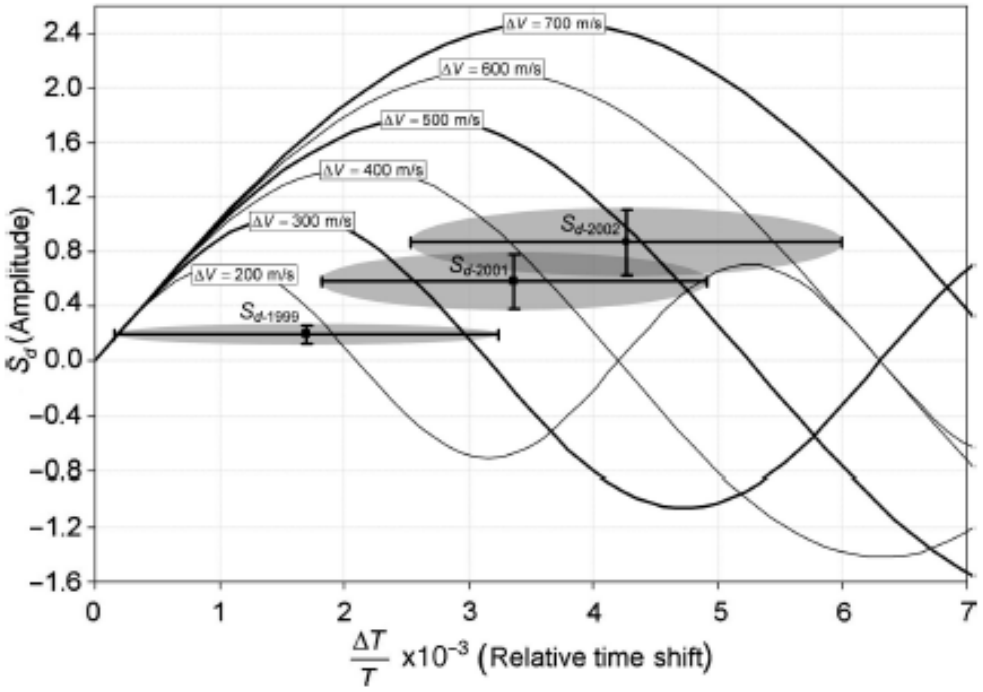

Figure 2.8: The results of studies conducted by Ghaderi & Landrø (2009) demonstrates the reflection amplitude as a function of relative time shift. The three points refer to their average measured amplitudes from the 1999, 2001 and 2002 monitoring datasets, whilst colored areas indicate spread in data measurements.

Table 2.1: Thickness variation in the CO2 containing layer estimated by combining reflection amplitudes and time-shift. Modified from Ghaderi & Landrø (2009).

Survey year	**ΔV (m/s)**	**Δz (m)**	**Δz CO_2 layer**
1999	200	15	4
2001	400	15	8
2002	500	15	10

The different models provide adequate descriptions of the CO_2 distribution. However, due to lack of knowledge about the actual gas saturation in each layer the velocity estimation includes significant uncertainties (Ghaderi & Landrø, 2009; Sturton et al., 2010). As signal attenuation gets more distinct with increasing quantities of gas present, a reduction in efficacy of seismic verification techniques is likely in future vintages. In addition, as the results are based on rock physics velocity models, the model uncertainty is substantial (Williams & Chadwick, 2012).

2.3.3 Layer thickness estimation by structural analysis

Concentrating about the uppermost mudstone layer, which is considered the main intra-reservoir unit to accommodate injected carbon dioxide, research has been done to find a relationship between the structural topography of the gas plume and layer thickness (Chadwick et al., 2009; Chadwick & Noy, 2010). The estimation indicates increasing CO_2 flux entering the uppermost layer. This suggests either an increase of migration with time or additional migration routes being established (Chadwick & Noy, 2010).

When estimating layer thickness based on structural analysis, the velocity model of overburden rocks is dependent on well data. In order to protect the sealing capacity of the cap rock above the reservoir, only two wells including necessary information are present close to the storage area - the deviated injection well and an appraisal well (Fornel & Estublier, 2013). Hence, a significant uncertainty is expected in the depth conversion of the model. Additionally, the number of migration pathways inserted in the model affects its certainty (Chadwick et al., 2009; Chadwick & Noy, 2010).

It is found that with a spacing less than 1/2 wavelength between two features in the subsurface, the producing reflections will interference with each other, and result in one single event of enhanced amplitude (Andreassen, 2009). The limit of 1/4 of the wavelength is called the tuning thickness of the seismic image. Below this limit, a single estimate of the layer thickness of subsurface elements from the seismic data becomes impossible. The research of Arts et al. (2004b) indicates a tuning thickness of about 8 meters for the intra-reservoir reflections in the Utsira reservoir. Attempting to improve the image of intra-reservoir layers with thicknesses below the tuning thickness, both pre- and post-stack inversion of time-lapse data has been conducted (Velis & Rubino, 2001; Delépine et al., 2001; Rubino & Velis, 2011). The method aims to characterize the spreading of CO_2 in the reservoir by estimation of the P-wave impedance. The approach is found to be useful for a quantitative in situ evaluation of carbon dioxide present in the reservoir.

2.3.4 Layer thickness estimation by geophysical methods

Aiming to estimate the carbon dioxide layer thicknesses, constrained AVO/AVA techniques has been applied with the purpose of estimating the thickness of individual CO_2 saturated layers (Buddensiek et al., 2010; Sturton et al., 2010; Rubino & Velis, 2011). By studying attenuation of seismic reflections and velocity changes as a result of injected CO_2, the research aimed its attention to how the velocity push-down effect due to carbon dioxide affected amplitudes as a function of its angle, and hence the seismic response of intra-reservoir layers containing CO_2.

The method resulted in a similar trend between the modeled and the actual dataset. However, the actual data has a significantly larger spread (Rubino & Velis, 2011). Further, the modeled data resulted in a leftward shift in comparison to the actual data. The results are therefore considered inconclusive (Williams & Chadwick, 2012).

Furthermore, layer thicknesses based on time-frequency analysis has by Williams and Chadwick (2012) been evaluated trough spectral decomposition, using the Wigner-Ville distribution. Despite the potential of this method, determining layer properties within the gas plume has proven to be challenging. Due to uncertainty in the interpretation of intra-reservoir layers as their spread is shown to be patchy and discontinuous, the technique is rather valid for the undoubted interpretation of the uppermost mudstone layer in the reservoir (Williams & Chadwick, 2012). As the velocity model is based on Gassmann's model with results highly sensitive to input properties, the excessive uncertainties of the model do not allow a specific conclusion to be made (Williams & Chadwick, 2012).

2.3.5 Property estimation by full waveform inversion (FWI)

Time-lapse full waveform inversion (FWI) has been applied to the dataset attempting to develop elastic parameter model both for the baseline dataset and for following monitoring datasets (Raknes et al., 2015). Synthetic models established based on the elastic parameters produces a good analog for events and discontinuity in the field data, and can thereby give an excellent demonstration of migration routes for the injected carbon dioxide in Utsira Formation (Raknes et al., 2015). Inverted models obtained from the baseline dataset and the monitoring dataset from 2006 gives clear indications of time-lapse anomalies and identifies at least four low-velocity layers surrounded by units generating higher velocities (Fig. 2.9). However, as the P-wave velocity changes due to gas injection can be immense, the misfit function for FWI might be subject to cycle skipping. Therefore, this technique alone might produce sufficiently reliable estimates of the true changes due to gas substitution in the Sleipner datasets.

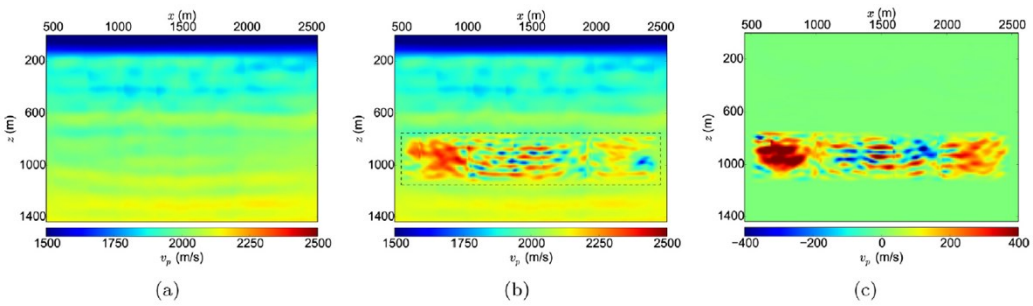

Figure 2. 9: Inverted models of a vertical slice using full waveform inversion (FWI) gives a clear indication of velocity anomalies. a) Baseline survey. b) Inverted model of the 2006 dataset. C) Time-lapse difference. From Raknes et al. (2015).

Chapter 3: Dataset and methodology

As the definition of a velocity analysis includes the distribution of signal velocities in a given region, velocity plays a significant role in seismic imaging with its main goal of producing high-quality images. Most estimation methods are based on kinematic changes in reflections. However, it is important to differ between methods based on measurements done in the data-domain and results of measurements done in the image-domain, as large variations will take place. The velocity analysis affects both the focusing of the data and determines the position of reflectors in physical space. Consequently, it is important to distinguish between the two components (1) focusing velocities affecting the focus of the seismic image and (2) depth consistency of the velocities affecting the position of reflectors. The ideal velocity model is the one that guarantees both the focusing and proper position of the reflectors in the seismic image. Due to the presence of noise and multiple reflections, there is no linear relationship between the focusing and depth errors in the image and the velocities. Therefore it is not straightforward to obtain the velocities/ or velocity changes directly from the seismic data. In general, the accomplishment of an appropriate model often requires additional information such as well data and geological models supplemental to the seismic time-lapse data.

Traditionally, velocity models are built by examining and determining the kinematics of reflections directly in the data-domain. Normally, this is done by iterative determination of the normal moveout (NMO) for different common mid-points (CMP) before applying the Dix formula to compute the interval velocity model used in the migration of the dataset.

In areas containing challenging geological structures and large lateral velocity variations, methods based on the data-domain often fail. Estimating velocities becomes in many cases both inaccurate and time-consuming. In these events, methods focusing on migration to extract kinematic information from the image-domain, known as migration velocity analysis (MVA), will both simplify the events and generate results that are more reliable. MVA is performed by imaging the prestack data, and then iteratively updating the velocity model based on the migration results (Sava, 2004). The method, as most velocity estimation processes, is dependent on the approximation used to determine the kinematic changes of different reflectors. Ray-based methods are beneficial as they are less time-consuming than extrapolating waves and as it provides a profound intuitive relation between the estimation of velocities and the kinematics of reflections.

However, in areas involving complex geology and sudden velocity changes, ray-based methods have their weaknesses. Wave-equation MVA is an approach applied in the image-

domain to extract a velocity model from the band-limited wave propagation. While conventional methods use space-lags or time-lags to produce common image gathers, the WEMVA procedure takes advantage of the coherency of reflections in extended images (Sava, 2004). Rather than measuring depth perturbations, WEMVA extracts image perturbations taking advantage of the full wavefield. By applying an inverted wave-equation operator, the image perturbations are converted into velocity perturbations. Hence, the WEMVA method is an adequate approach for areas containing a complex subsurface environment. As the goal of the estimation is to maximize the quality of the image, wavefield-extrapolation methods should be considered in areas where the velocity function is highly sensitive to spatial variations in topography and/or fluid content, such as the case of carbon dioxide injection.

As the MVA method aims to linearize the wave-equation based on the scattering theory of the Born approximation (Pratt, 1999; Dahlen et al., 2000), challenges develop when the phase of the model and the recorded wavefield are larger than a fraction of the wavelet. Under these circumstances, the assumption of the Born approximation is violated. One way to overcome this problem is to limit the frequency of the wavelet used in the analysis.

3.1 Dataset and processing steps

To follow the Sleipner injections and its behavior over a period of time, the monitoring data in this thesis have been constrained to include 3D seismic datasets acquired in 1994, 2001 and 2006 obtained the Sleipner storage facility located in the central North Sea (Fig. 3.1), with 0 Mt, 4.20 Mt and 8.40 Mt injected CO_2, respectively. The 1994 dataset was acquired before injection and will, therefore, be referred to as the baseline survey. As this study aims to detect the velocity changes in a time-lapse survey due to differences in fluid saturation, acquisition

repeatability is important. Key acquisition parameters are listed below (Tab 3.1). All datasets are displayed with negative polarity.

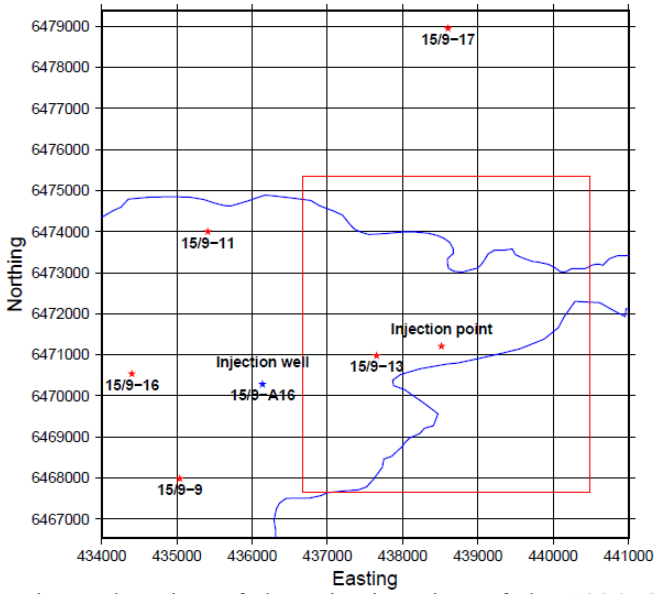

Fig. 3.1: Approximate location of the seismic cubes of the 1994, 2001 and 2006 seismic surveys is marked with a red. In addition, the location of wells drilled nearby the study area is marked with red stars. The blue star of well 15/9-A-16 refers to the injection well.

Table 3.1: Key acquisition parameters for the seismic surveys implemented in this study. Modified from Chadwick et al. (2008).

Survey	**ST9407**	**ST0106**	**ST0607**
Data acquired	06.08-10.09.1994	27.09-01.10.2001	June 2006
Shooting direction	0.853 degrees	0.850 degrees	0.850 degrees
Source tow depth	6 m	6 m	6 m
No. of sub arrays	3	3	3
Source x-line separation	50 m	50 m	50 m
Source volume	3400 in^3	3397 in^3	3660 in^3
No. of sources	2	2	2
Shot point interval	18.75 m	12.5 m	18.75 m
No. of cables	5	4	8
Cable separation	100 m	100 m	100 m
Cable length	3000 m	1500 m (3000 m)	3600 m
Near offset	195 m	150 m	130 m
Group interval	12.5 m	12.5 m	12.5 m
Tow depth	8 m	8 m	8 m
CO2 content in reservoir (Million tonnes Mt)		4.20	8.40

Before issuing the data, the contractor applied following processing steps:

1. Restricted maximum offset to 1700 m,
2. Reduced the recording length to 2.3 s,
3. Applied a signature deconvolution and swell noise filter,
4. Applied a low-cut filter at 6.0 Hz,
5. Sampled the time-step to 2.0 ms and,
6. Gained the data using a t^2 scaling factor.

Processing of all datasets was done using Halliburton's SeisSpace ProMAX Seismic Processing Software. To ensure a satisfying foundation for the velocity analysis, an identical bin-size, corresponding to 12.5x25, was set for all datasets. As a result, the baseline survey obtained a maximum fold of 120, with an average fold of 55. The 2001 and 2006 datasets were given a maximum fold of 190 and 130, and an average fold of 100 and 65, respectively. In order to compensate for the loss of amplitudes due to wavefront spreading, a spherical divergence correction was performed based on interval velocities extracted from well 15/9-9 drilled in 1981 – before injection (Fig. 3.2; Arts, 2000).

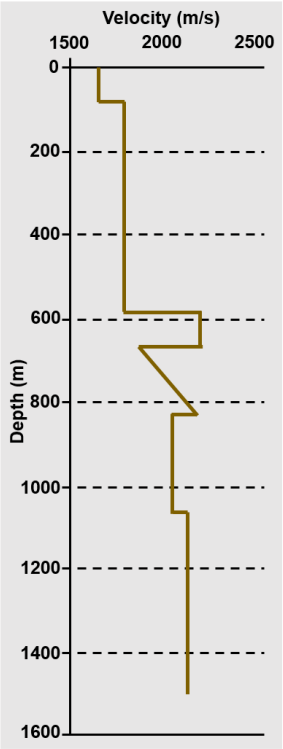

ig. 3.2: Interval velocities based on well 15/9-9 applied for the spherical ivergence correction. Modified from Arts (2000).

A baseline velocity stacking model was produced from velocity analysis of the baseline survey. Velocities were manually picked for every CDP derived from a supergather combining 3 in-lines and 5 cross-lines. Further, an NMO-correction using 95 % of the velocity model was run on the baseline dataset in order to manufacture an FK-polygon used to filter out multiples. Furthermore, a new velocity model was created by manually picking velocities from each CDP using data with a distinct decrease in multiples in order to enhance the certainty of the model (Fig. 3.3a).

Accordingly, an NMO-correction using the new velocity model was applied to all dataset before implementing a vertical stack algorithm which sums the sample values contributing to each CMP before dividing these by the number of samples summed, raised to a supplied power 0.5. Additionally, post-stack phase shift migration was applied to handle lateral velocity variations by time stretching seismic traces to approximate traces using an interval velocity model converted from the original baseline velocity model (Fig. 3.3b). Regarding the baseline survey, Ormsby bandpass filter was applied after the migration process to attenuate noise. The four corner frequencies (frequency-slope-frequency-slope) was set to 3-8-120-130 Hz.

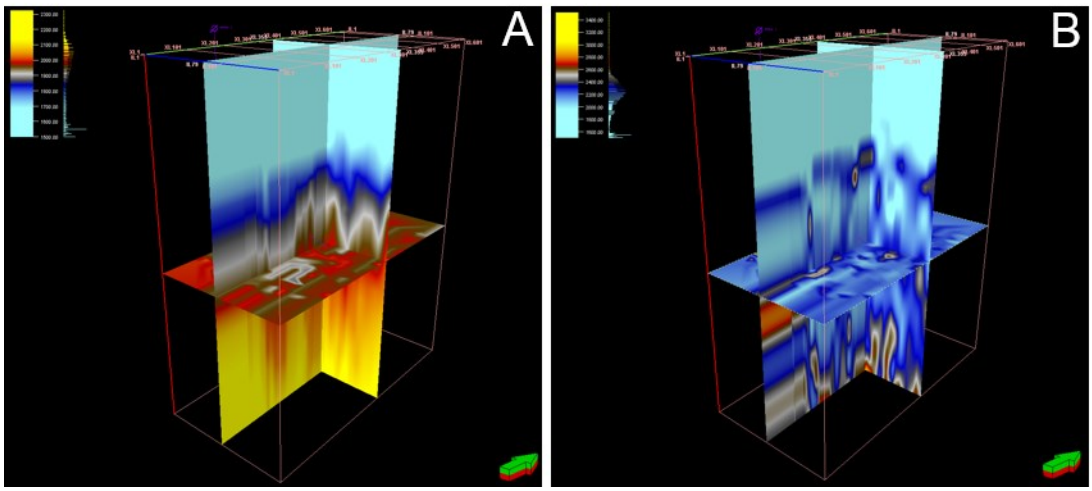

Fig. 3.3: A) Manually picked RMS velocity model based on the pre-injection baseline survey. B) Interval velocity model converted from the original RMS velocity model.

Main horizons were manually interpreted by the use of Schlumberger's Petrel E&P Software Platform. As the overlying Hordaland Group is consisting of shale with a higher impedance than the sandstone reservoir, and based on the polarity of the datasets, the upper boundary of Utsira Formation was interpreted as an amplitude peak in the datasets corresponding to standard seismic reflection theory (Eq. 3.1). Consequently, the lower boundary of the reservoir was interpreted as a trough. Supplementary to the time-lapse surveys analyzed, well data from well 15/9-9, 15/9-11 and 15/9-13 was provided to ensure an accurate

interpretation of these key horizons. Even though all wells are located outside the area of the plume (Fig. 3.1), the wells penetrate Utsira Formation as well as the over- and underlying formations making the data applicable for this study. Following, intra-reservoir mudstone layers was interpreted as negative reflectors. As a result of an excessively strong reflector for the uppermost shale layer and accordingly intra-reservoir multiples, it was only possible to interpret with certainty five isolated shale units.

$$R = \frac{V_2\rho_2 - V_1\rho_1}{V_2\rho_2 + V_1\rho_1} \tag{3.1}$$

Interpolation of surfaces from the interpreted horizons was conducted using MathWorks MATLAB software with courtesy of Assoc. Prof. Wiktor W. Weibull (Appendix A). To reduce travel time fluctuations as a result of local noise, the interpolated values was smoothed using a spatial filter. When creating a plume model containing the interpreted flow units including carbon dioxide, the gas layer thicknesses was set to 40 ms (Appendix A). With an average velocity of 2000 m/s, this equals to 40 meters thick gas layers. Choosing a larger layer thickness caused individual events to merge with each other. This is a contradiction to what is observed in the seismic data. Hence, the thickness of 40 meters was considered an appropriate initial guess to the size of the gas column.

The different vintages (1994, 2001 and 2006) have significant differences in source signature and acquisition parameters. In order to compensate for the mismatch between the different datasets, the 2001- and 2006-datasets were time-shifted with -5.24 ms and -9.73 ms, respectively. The time-shift measurements were determined by defining a polygon outside the area affected by the gas injections on the upper boundary of Utsira Formation and establishing the mean difference in interpreted horizons. The time-shift value was set to be constant for all interpreted horizons in the 2001- and 2006-datasets to match the baseline survey.

3.2 RMS minimum amplitude

In order to map the carbon dioxide plume in the Utsira Formation, post-stack root-mean-square (RMS) amplitude attribute was implemented on all datasets with a window constrained by the interpreted top and base of the Formation. As the attribute measures and emphasizes the magnitude of variation in reflectivity and acoustic impedance, the method is considered a direct hydrocarbon indicator (Chopra & Marfurt, 2005; Nanda, 2016). By using equation 3.2 squared amplitudes based on their relative weight are summed before divided by the total weight of all amplitudes in the focusing window. The attribute gives an indication of the lateral extent of the plume and provides an implication of its development. The RMS amplitude attribute was

applied on smoothed surfaces in Petrel. With n indicating the number of samples, Amp referring to the amplitude and w being the weight of each amplitude, the RMS amplitude was calculated as follows:

$$RMS_{Amplitude} = \sqrt{\frac{\sum_{i=1}^{n} Amp_i^2 * w_i}{\sum_{i=1}^{n} w_i}} \tag{3.2}$$

3.3 Velocity estimation using wave-equation migration velocity analysis

In order to translate the difference in depth of the base of the reservoir to changes in seismic velocities, a tomographic method must be used. Image-domain tomographic methods, such as wave-equation migration velocity analysis, is a suitable method to apply for the improvement of velocity models extracted from the seismic data (Sava, 2004; Sava & Biondi, 2004; Shragge & Lumley, 2013). Target image fitting exploits the deviation between the insufficient depth migrated image and a perfectly focused version of the data. Working with time-lapse seismic data including a different amount of injected gas, the reflector location on the baseline survey will be considered the perfectly focused version of the subsurface image, and hence will be the objective when updating the monitoring vintages.

The WEMVA-method have originally been designed to improve the focusing of the seismic data in the image-domain. However, the method can be modified to deal with time-lapse datasets without the need for modifications to its main components, except for the description of the objective function (Shragge & Lumley, 2013). The WEMVA operator consists of three main elements; (1) building a background wavefield, (2) the evaluation of the forward operator and (3) the assessment of the adjoint WEMVA operator (Fig. 3.4). In a non-linear implementation of WEMVA, these elements are iterated until a convergence criterion is reached by the use of the open-source Madagascar software.

The wave-equation migration velocity analysis performed in this contribution is based on the theoretical work of Sava (2004) and Sava & Biondi (2004). The operator notations are adopted from Shragge & Lumley (2013).

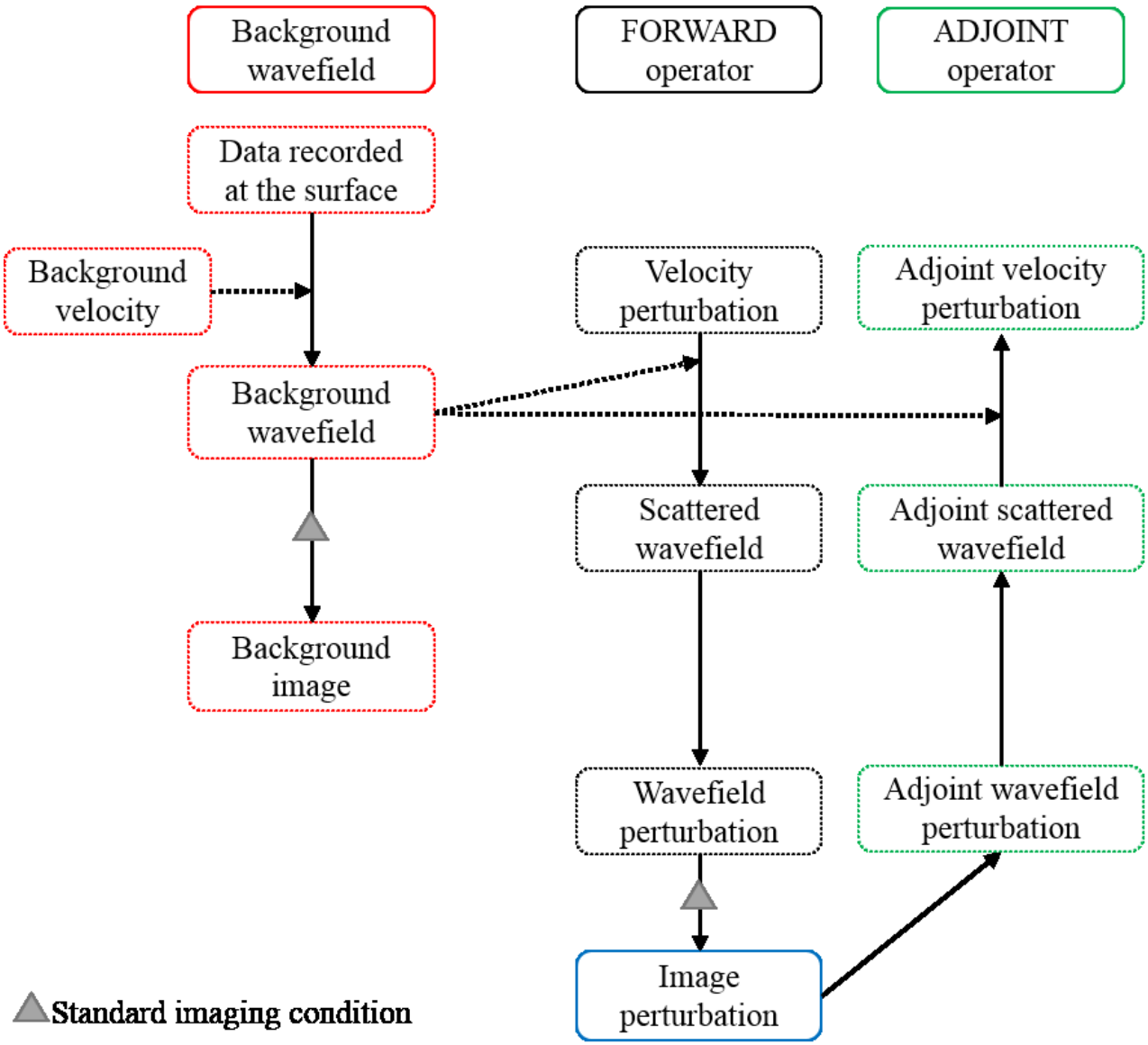

Fig. 3.4: Schematic illustration describing the process of updating the velocity model based on migration results. The three main elements of the process are (1) building a background wavefield, (2) the evaluation of the forward operator and (3) the assessment of the adjoint WEMVA operator.

3.3.1 WEMVA operator

Conventional wave-equation seismic modeling operators (F) relates an acoustic model of the subsurface (m) to the measured dataset (d), and construct an adjoint operator ($F^{\ddagger}$) applied to manufacture a model image (I_m):

$$Fm = d \tag{3.3}$$

$$F^{\ddagger}d = I_m \approx \mathrm{m} \tag{3.4}$$

The development of the WEMVA operator is based on the migration and adjoint migration operators L_{V0} and $L_{V0}^{\ddagger}$, respectively, where the true background velocity model (V_0) is incorporated. Implementing the migration operator on the true subsurface image (I_0) will result in the recorded dataset (Eq. 3.5). Correspondingly, applying the migration operator to the dataset (d) will reproduce the true image (Eq. 3.6).

$$L_{V0} I_0 = d \tag{3.5}$$

$$L_{V0}^{\ddagger} d = I_0 \tag{3.6}$$

The background wavefield model is constructed based on the data recorded at the surface. By using the background velocity model and applying methods like generalized screen propagator, Fourier finite-difference or finite difference modeling of the two-way acoustic wave-equation to the source wavelet and recorded data, the wavefield can be predicted for all depths (Sava, 2004). Since the extrapolated wavefield contains crucial information about the wave paths in the subsurface, where velocity errors are determined, this component is fundamental for the WEMVA operator. Using standard imaging conditions with the background wavefield model, the result will provide the background image.

Theoretically, by using the true velocity model (V_0), a perfect, bandlimited image of the subsurface can be retrieved (Shragge & Lumley, 2013). However, in practice, only an estimation of the background velocity model (V_1) can be estimated from the dataset, resulting in an approximately optimal image (I_1) of the subsurface (Eq. 3.7).

$$L_{V1}^{\ddagger} d = I_1 \tag{3.7}$$

As the resulting image is based on an estimated background velocity, it is known that $I_0 \neq I_1$. Simultaneously, the argument $V_0 \neq V_1$ is established. By determining the difference between the estimated background velocity model and the true velocity model ($\Delta V = V_0 - V_1$), and using ΔV in equation 3.5, the result will produce the difference in data volume Δd:

$$L_{\Delta V} I_0 = [L_{V0} - L_{V1}] I_0 = d_0 - d_1 = \Delta d \tag{3.8}$$

Subsequently, the adjoint migration operator implemented with ΔV and applied on the recorded data will produce the perturbed image volume ΔI:

$$L_{\Delta V}^{\ddagger} d = [L_{V0} - L_{V1}] d = I_0 - I_1 = \Delta I \tag{3.9}$$

By this means, the inversion objective is to define a background perturbation velocity model (ΔV) which is designed to sufficiently demonstrate the perturbed image volume (ΔI). As

the operator is depends on the nonlinear ΔV model, the inversion objective likewise will be nonlinear. Despite the fact that a nonlinear solution is possible (Girard & Vasconcelos, 2010; Yang & Sava, 2011), the scattering theory used in this assessment of the forward operator is based on the Born approximation (Born, 1926; Pratt, 1999; Dahlen et al., 2000). The Born approximation is restricted to situations where the scattered field is limited compared to the incident field of scatter. Since the scattering appears independently at different elevations, the approximation is suitable for the WEMVA method. However, preventative measures must be taken to avoid cycle-skipping difficulties. These complications can be overcome by linearizing the image perturbations (Sava, 2004; Sava & Biondi, 2004), or as it is done in this study, by choosing a wavelet with low enough frequency as to keep the image perturbations less than the one-quarter of the wavelength of the seismic data.

To define a linear relation between the background perturbation velocity volume ΔV and perturbed image volume ΔI, the theoretical methodology of Sava & Biondi (2004) will be followed. For this purpose, a WEMVA forward and adjoint operator, $T_{d,v0}$ and $T_{d,v0}^{\ast}$, respectively, is introduced (Eq. 3.10; Eq. 3.11). The notation d,v_0 implies that the operator integrated with the true background velocity model V_0 is applied to the dataset d. In the assessment of the forward operator, the combination of the background wavefield and the velocity perturbation is used to develop an estimation of the scattered wavefield. Applying an equal numerical integration as when extrapolating the background wavefield, the total scattered wavefield, referred to as the wavefield perturbation, is estimated for all depth levels in the model. Hence, the wavefield perturbation at any level sums the scattering effects of all levels above (Sava, 2004). Accordingly, the wavefield perturbation implemented with standard imaging conditions will result in a perturbation image comparable to the interaction between the background wavefield and the velocity perturbation (Sava, 2004).

$$T_{\mathrm{d,V0}}\Delta \mathrm{V} = \Delta \mathrm{I} \tag{3.10}$$

$$T_{\mathrm{d,V0}}^{\ast}\Delta I = \Delta \mathrm{V} \tag{3.11}$$

The adjoint operator is representing the inverse process of the forward operator, where the velocity perturbation model is assembled from the image perturbation. Implementing an adjoint imaging operator to the image perturbation, an adjoint wavefield perturbation can be developed (Sava, 2004). Thereby enforcing the adjoint wavefield perturbation to all depth levels, the adjoint scattered wavefield is established. Subsequently, by implementing the background wavefield, the adjoint velocity perturbation can be produced. The key reflectors on

the monitor surveys are then iteratively matched to the equivalent reflectors interpreted in the baseline survey by tomographically updating the velocity model. For a more thorough mathematical description of both the forward and the adjoint operator, readers are referred to Sava & Biondi (2004).

By combining the forward and adjoint operators (Eq. 3.10; Eq. 3.11), together with weighted velocity model (W) used to set the boundaries for tomographic updates in the dataset, a WEMVA operator (τ) is established:

$$\tau = \frac{1}{2}\left|\mathrm{W}\left(\mathrm{T}_{\mathrm{d,S0}}\Delta\mathrm{V} - \Delta\mathrm{I}\right)\right|^2 \tag{3.12}$$

3.3.2 Time-lapse wave-equation migration velocity analysis

When considering time-lapse surveys with increasing injection of carbon dioxide, as for the Sleipner field, for the WEMVA method, the alteration in properties within the subsurface must be considered. Hereby, the baseline survey will be referred to as d_1, while the monitoring dataset will be named d_2. With the alteration of subsurface properties, the background velocity model will adjust. Accordingly, the alteration introduces at least three different estimation objectives for the time-lapse wave-equation migration velocity analysis: (1) the difference between the baseline (S_1) and the true background (V_0) velocity models (Eq. 3.13), (2) the difference between the monitor (V_2) and the true background (V_0) velocity models (Eq. 3.14), and (3) the difference between the baseline (V_1) and the monitor background (V_2) velocity models (Eq. 3.15).

$$\Delta\mathrm{V}_1 = V_1 - V_0 \tag{3.13}$$

$$\Delta\mathrm{V}_2 = V_2 - V_0 \tag{3.14}$$

$$\Delta\mathrm{V}_{1,2} = V_2 - V_1 \tag{3.15}$$

Theoretically, the difference in data volume when considering a baseline and a monitor survey is affected only by the manufactured change of the subsurface as a result of CO_2 injections. Nonetheless, as repeating the exact acquisition conditions for all surveys is impossible due to the presence of coherent noise, the notations σ_1, σ_2, and $\sigma_{1,2}$ is introduced to represent measurement errors. As a result, the objectives than can be described as:

$$\tilde{\mathrm{V}}_1 = \Delta\mathrm{V}_1 + \sigma_1 = V_1 - V_0 + \sigma_1 \tag{3.16}$$

$$\tilde{\mathrm{V}}_2 = \Delta\mathrm{V}_2 + \sigma_2 = V_2 - V_0 + \sigma_2 \tag{3.17}$$

$$\tilde{V}_{1,2} = \Delta V_{1,2} + \sigma_{1,2} = V_2 - V_1 + \sigma_{1,2} \tag{3.18}$$

This analysis will primarily pursue the latter objective (Eq. 3.18). The time-lapse WEMVA approach is performed by applying the 3D WEMVA operator separately to both the baseline (d_1) and the monitor (d_2) dataset:

$$\tau_1 = \frac{1}{2}\left|W\left(T_{d1,V0}\Delta V_1 - \Delta I_1\right)\right|^2 \tag{3.19}$$

$$\tau_2 = \frac{1}{2}\left|W\left(T_{d2,V0}\Delta V_2 - \Delta I_2\right)\right|^2 \tag{3.20}$$

In addition, enforcing the tomographic operator, the difference in image perturbation volume ($\Delta I_{1,2} = I_2 - I_1$) can be determined. Thus, approaching the same argument as for the 3D WEMVA modeling operator, a time-lapse wave-equation migration velocity analysis operator can be appointed to reach the analysis objective, $\tilde{V}_{1,2}$.

$$\tilde{V}_{1,2} = \operatorname{argmin}_{\Delta V1,2}\left[\tau_{1,2}\right] = \operatorname{argmin}_{\Delta V1,2}\left[\frac{1}{2}\left|W\left(T_{d,v}\Delta V_{1,2} - \Delta I_{1,2}\right)\right|^2\right] \tag{3.21}$$

Finally, the determined velocity model $\tilde{V}_{1,2}$, and in its turn $\tilde{V}_{1,3}$ for the latter monitor dataset, will be implemented in the forwarding operator in order to migrate the different images of the subsurface on the monitor datasets according to the baseline interpretation.

Chapter 4: Results

4.1 Interpreted horizons

Based on 3D seismic surveys, top and bottom boundaries of the Utsira Formation were interpreted on all vintages (Fig. 4.1). In addition, five different intra-reservoir horizons were interpreted on the seismic surveys conducted in 2001 and 2006 (Fig. 4.1). Carbon dioxide is injected at the base of Utsira Formation at a depth of 1164 meters for storage. An easily seen vertical feature identified by the distinguished push-down effect below and attenuating reflection amplitudes is characterized as a chimney and a major vertical migration pathway for the CO_2 (Fig. 4.1). Hence, injected gas is transported from the injection point close to the Utsira lower boundary towards the shallowest part of the reservoir, with local trapping mechanisms located with different depths (Fig. 4.1).

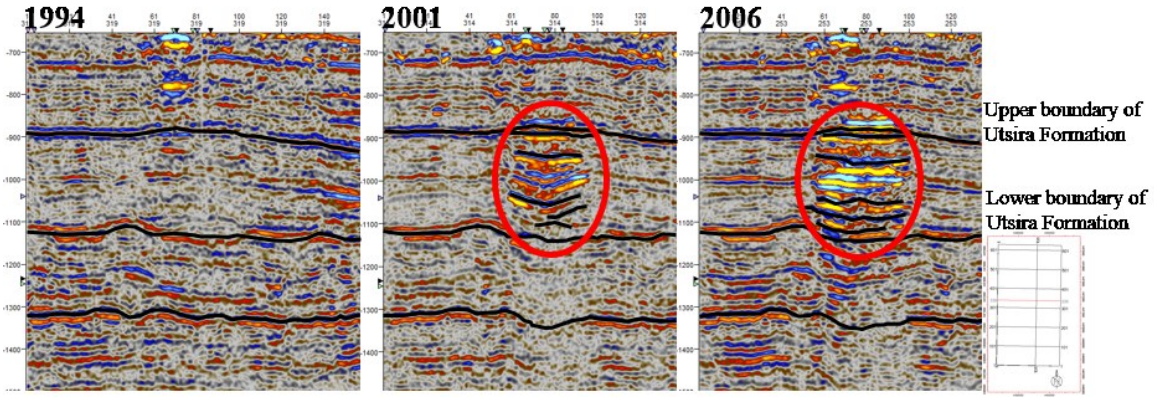

Fig. 4.1: Figure displaying key reflectors interpreted on thecorresponding cross-line in the 1994, 2001 and 2004 dataset. Both intra-reservoir mudstone layers, upper and lower boundary of the reservoir, and a reflection below the reservoir is interpreted. Chaotic reflections (red circle) is visible in the center of the reservoir due to gas injection characterized as a chimney structure and migration route from the injection point towards the more shallower parts of the reservoir.

The boundary between the top of the Utsira sands and the overlying shales of the Nordland group was interpreted as a strong positive reflector. The depth of the boundary is ranging between 865 and 900 ms, which after the conducted depth-conversion ranges between 800 and 900 meters, on the baseline dataset (Fig. 4.2). The interpretation is considered as the upper boundary of the reservoir and hence the shallowest point of storage for the injected carbon dioxide. The interpreted surface has a topographic ridge structure, with a reducing relief towards the southern part (Fig. 4.2). The wedge measures approximately two km in width in

the widest part. However, at the site of injection, the topographical structure is measured to only ~700 meters in width at the injection site.

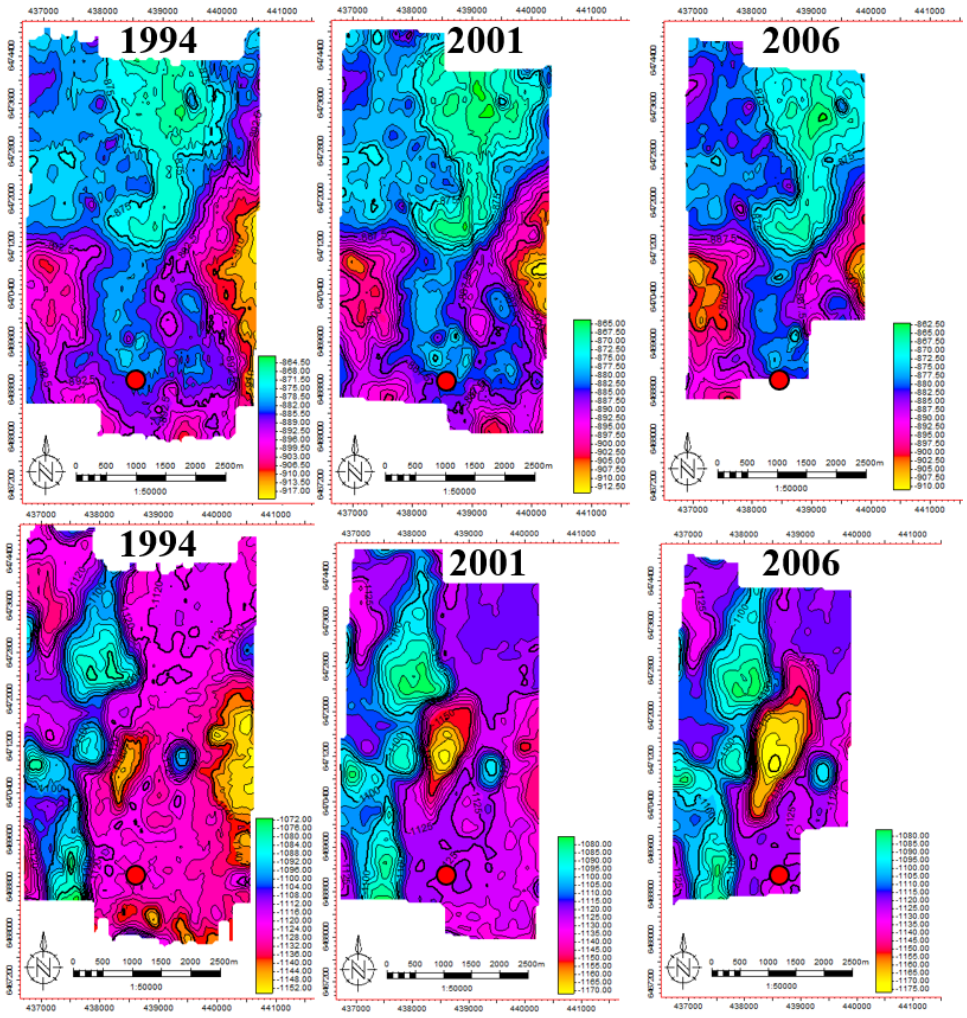

Fig. 4.2: Structural maps as a function of two-way time indicating architectural tendency of the upper (upper column) and lower (lower column) boundary of the Utsira Formation for each vintage. The red disc illustrates the injection point of carbon dioxide.

The base of Utsira was interpreted as a negative reflector at a depth of approximately 1070 to 1150 ms and 1100 to 1200 meters on the baseline dataset (Fig. 4.2). As a result of mud volcanoes present, the reflector is not absolutely continuous. Nonetheless, a reasonable interpretation was made based on a combination of all vintages. The interpretation was validated in comparison with well data from well 15/9-13. The topography of the reservoir base is relatively flat. However, a saddle-like structure is seen extending from the northwestern to the southwestern part of the surface (Fig. 4.2). In addition, the interpretation exposes a natural depression as the base boundary located directly to the north of the injection point. Later vintages display a growing depression. Assuming that the depth of the Utsira base, and hence the formation thickness, does not differ due to the injection, this development is a direct result of the velocity changes due to the increase in gas saturation.

Five intra-reservoir mudstone layers were interpreted on the 2001 and 2006 seismic surveys. Due to weak reflectors in the 1994-dataset, it was not possible to interpret these layers with certainty in this dataset (Fig. 4.3). As a result of injected CO_2 and its impact on the seismic signal, the shale layers is possible to interpret as negative amplitude anomalies on the seismic image (Fig. 4.1). The shale layers have a relatively flat topography. The 1st layer has a small topographic high towards the reservoir center, while the remaining layers include a small topographic low towards the injection point (Fig. 4.3). A lateral growth of reflectors representing the shale layers is observed moving from the 2001 to the 2006 dataset (Fig. 4.1; 4.3).

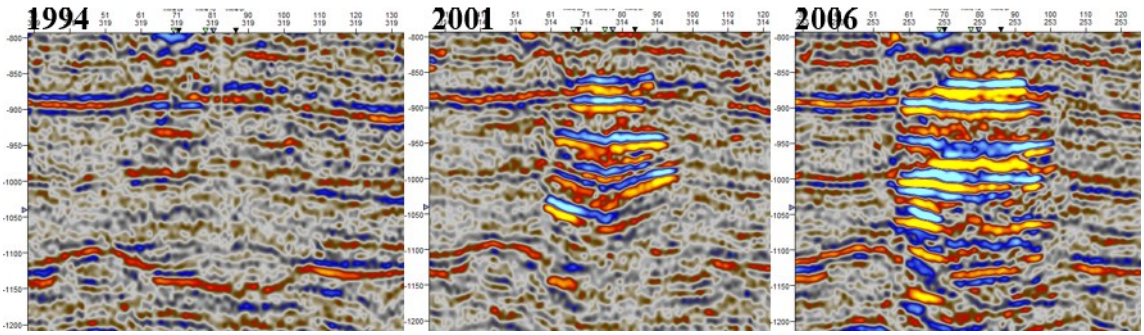

Fig. 4.3: Seismic images of the both the base and the monitoring surveys giving a clear indication of how the negative amplitudes increase with the injection of gas on monitoring surveys.

From well logs, nine to twelve shale units are interpreted. Only five of these layers are mapped out in the monitoring seismic image due to the patchy extent of the layers. In addition, a strong multiple of the upper boundary reflector develops due to the enhanced reflection coefficient of the boundary following the increased gas saturation (Fig. 4.1; 4.3). Hence, an interpretation in the area of the multiple reflectors could not be determined with sufficient certainty and was therefore not included in this study.

4.2 Mapping of the CO_2 plume from time-lapse seismic data

As a result of the injection, the tuning thickness of the intra-reservoir layers is observed to increase (Fig. 4.3). Accordingly, the seismic image indicates a decreasing vertical resolution of the seismic image with the increasing amount of gas present. Easily detected, intensified seismic amplitude anomalies has been developed on later vintages corresponding to carbon dioxide stored in the reservoir, while few amplitude anomalies are observed at the baseline survey (Fig. 4.3). As the baseline survey was conducted pre-injections, the data contains the mudstone layers only. With no energy implemented by the present of CO_2, the very thin shale layers do not reflect enough energy to be distinguishable.

RMS minimum amplitude maps were considered a good approach to determining the plume structure development. From the RMS map, a clear elliptical shape with the long axis in the NNE-SSW direction and the short axis in the WNW-ESE direction is revealed (Fig. 4.4). By measuring the length of both axis (Tab. 4.1), more than 40 % growth in the long axis is seen from 2001 to 2006. In contrast, only 13 % growth in the short axis is measured.

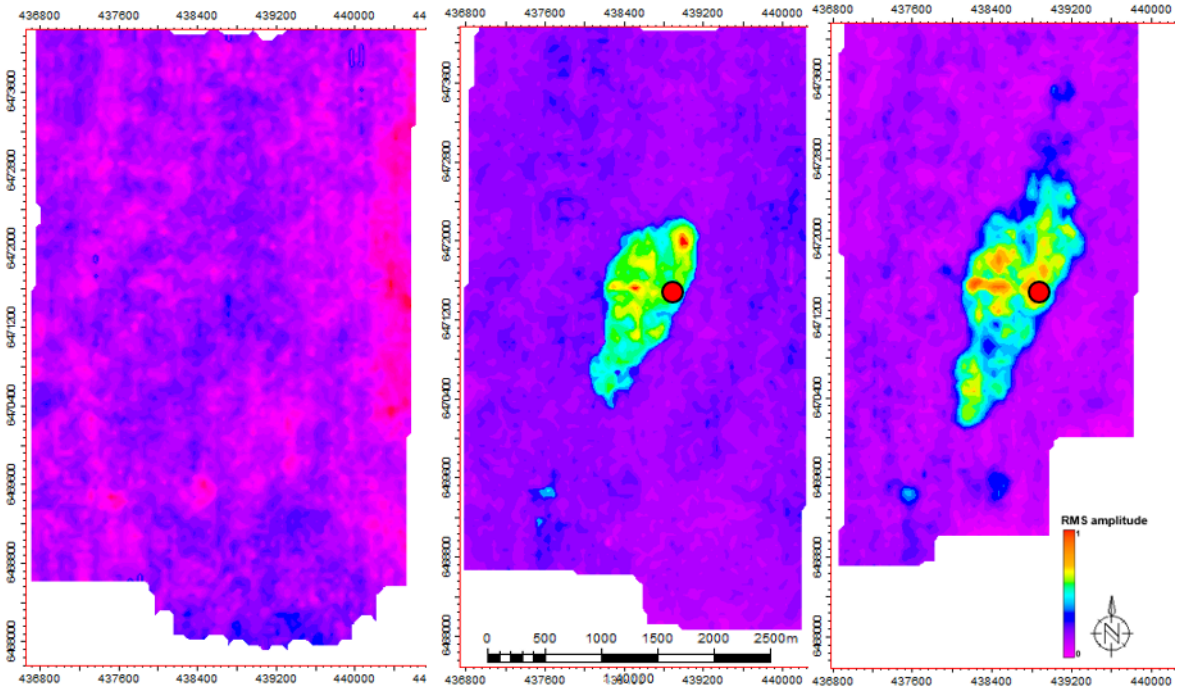

Fig. 4.4: RMS minimum amplitude maps for each vintage illustrates the lateral shape of the reservoir with a shape with an NNE-SSW direction of the long axis a WNW-ESE direction of the short axis. The red disc represents the point of injection.

Table 4.1: Measurements from RMS minimum amplitude maps for each survey (Fig. 4.4).

Survey	**ST9407**	**ST0106**	**ST0607**
Data acquired in	October 1994	October 2001	June 2006
Length long axis	N/A	2000 m	3600 m
Length short axis	N/A	800 m	920 m

4.3 Velocity changes estimated based on target image fitting

Wave-equation migration velocity analysis is a method based on target image fitting. Target image-fitting exploits the depth difference of a particular reflector or reflectors in two different migrated images of the same area. For this study, the reflector representing the base of the Utsira formation, interpreted from the baseline pre-injection image is assumed to be at the correct depth. This reflector is demigrated and remigrated using the initial velocity model obtained from the 1994 data, and the resulting image was considered the "target image" for this reflector (Fig. 4.5). The same reflector was interpreted in both the 2001 and 2006 vintages. The velocity model of the monitoring datasets was updated aiming to relocate the equivalent interpreted key reflectors to the match the depth of the target image. Two different velocity updates were produced using different constraints on the velocity updates. In the first attempt, the velocity updates were limited to the pre-determined location given by both the upper and the lower boundary of the reservoir (Fig. 4.6a). In a second attempt, the velocities are constrained to the approximate location of gas accumulation below intra-reservoir sealing units (Fig. 4.6b, c).

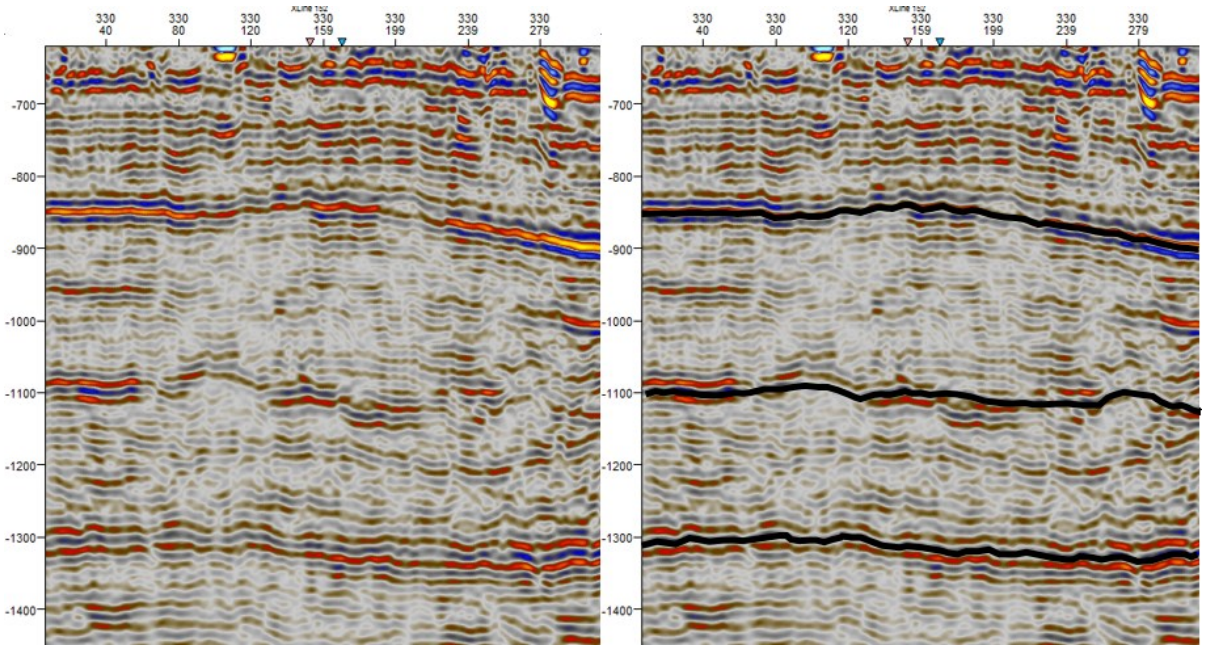

Fig. 4.5: A migrated image of the baseline survey determining the location of key reflectors in depth. Both the upper and the lower boundary is interpreted. In addition, a prominent reflector below the reservoir is interpreted.

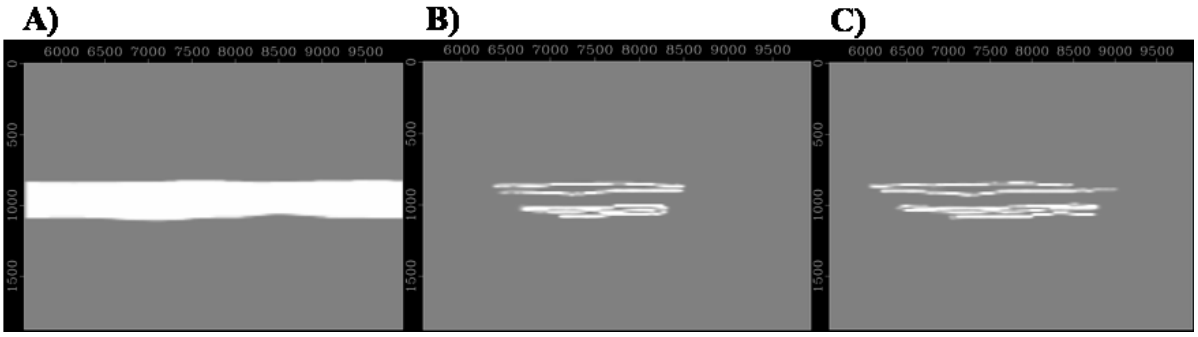

Fig. 4.6: The constraints set for each velocity model. A) The velocity model constrained to only the top and base reflector of the reservoir is based on this model. B) An indication of the intra-reservoir gas accumulations where velocity changes are determined to take place in the plume model for 2001. C) An indication of the intra-reservoir gas accumulations where velocity changes are determined to take place in the plume model for 2006.

Figure 4.7 illustrates the pre-migrated interpretation of horizons indicating the Utsira base reflector of all datasets. A distinct push-down effect is seen in the post-injection reflections. Demigrating these reflectors with a wavelet of predetermined frequency, and using the velocity model of the baseline data and the respective acquisition geometry of each dataset, synthetic data is created for each reflector. Then by the process of target image fitting, the velocities for each dataset are iteratively updated, until the images of the reflectors representing the base Utsira formation in the monitor surveys match in depth with the "target reflector," from the baseline survey. To avoid cycle skipping in the target image fitting procedure, the frequency of the wavelet is chosen such that the maximum depth difference between the reflectors is less than a quarter of the wavelength of the seismic data. This guarantees convergence to the global minimum in the optimization procedure.

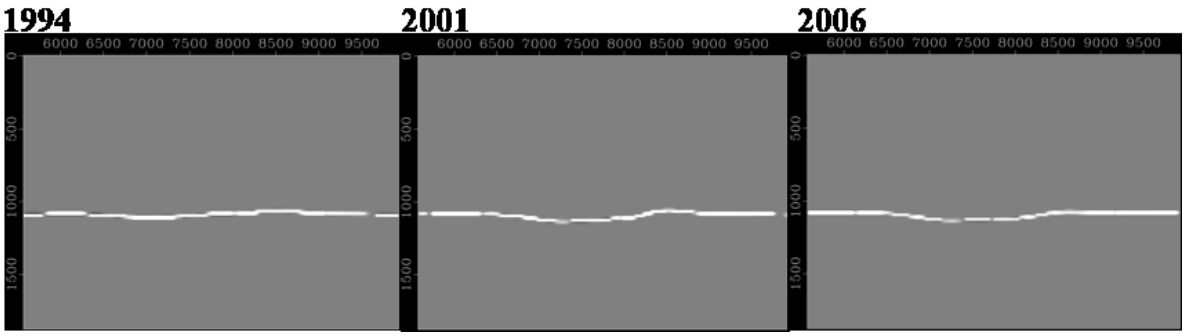

Fig. 4.7: Unmigrated interpretation of base horizons in each dataset. The velocity model developed with the WEMVA method aims to relocate horizons of the monitoring datasets to match the depth of the baseline survey of 1994.

When updating the velocity model constrained by top and base reflectors, velocity decrease due to the gas saturation is uniformly spread out over the reservoir formation (Fig. 4.8; 4.9). The model was iteratively updated aiming to migrate the base reflector of the reservoir to match the location of the corresponding reflector of the baseline model. Three iterations were conducted for the 2001 monitor dataset (Fig. 4.8), while only two iterations were conducted for the 2006 monitor dataset (Fig. 4.9). However, updating the velocity model for the 2001 monitoring dataset a distinct difference is visible between the first and the second iteration (Fig. 4.8). As the contrast between the second and the third iteration is rather insignificant, the resulting velocity model of the 2006 monitoring survey is considered adequate. The velocity models have a clear indication of noise illustrated as high-velocity fields on the edges of the gas reservoir in the Utsira layer (Fig. 4.8; 4.9). This effect is caused by the edges effects due to the limits imposed to save both processing time and computer memory. The effect was not corrected for due to time constraints. However, correcting for the edge-effect on the velocity model will have no effect on the migrated image of the center reservoir.

A second velocity model, which constrained the velocity changes to the accumulated carbon dioxide beneath the intra-reservoir shales, was iteratively updated for both monitoring datasets (Fig. 4.10; 4.11). This model indicates local areas of velocity decrease which will affect the migrated image. Apart from the velocity field within the reservoir affected by gas injections, all velocity models, independently of their constraints, has an identical expression directly above the Utsira sand package. This as a result of equal constraint based on the interpreted reservoir upper boundary put on all velocity models.

A velocity increase is as expected distinguishable for both the overlying Nordland shales and the underlying Hordaland shales. The abundant velocity increase at a depth of ~1500-2000 meters is a result of decreasing resolution with depth for all surveys. The effect is a direct consequence of the initial velocity model, which was manually picked from pre-injection pre-stacked CDPs. As this study has concentrated on the migrated image at a shallower depth, the certainty of the initial velocity model was mainly focused on the carbon dioxide reservoir and its effect on the velocities.

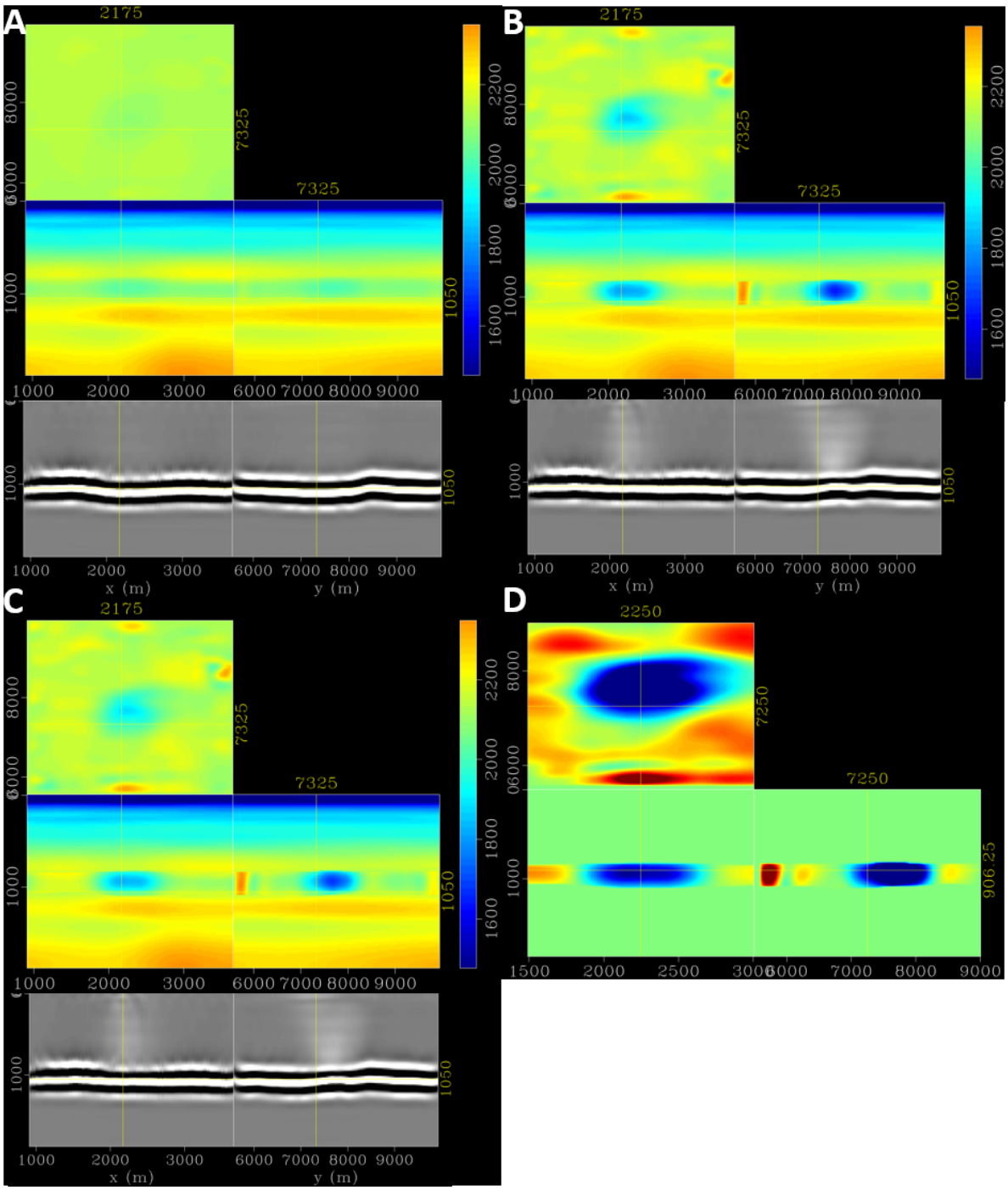

Fig. 4.8: The velocity model for the 2001 monitoring survey, with constraints of the upper and lower boundary of the reservoir (Fig. 4.8a). A, B and C represents the velocity model after one, two and three iterations, respectively. The velocity models are used to migrate the Utsira base reflector illustrated below each model. X, Y and Z coordinates are given in meters. D illustrates the difference between the final velocity model and the initial velocity model.

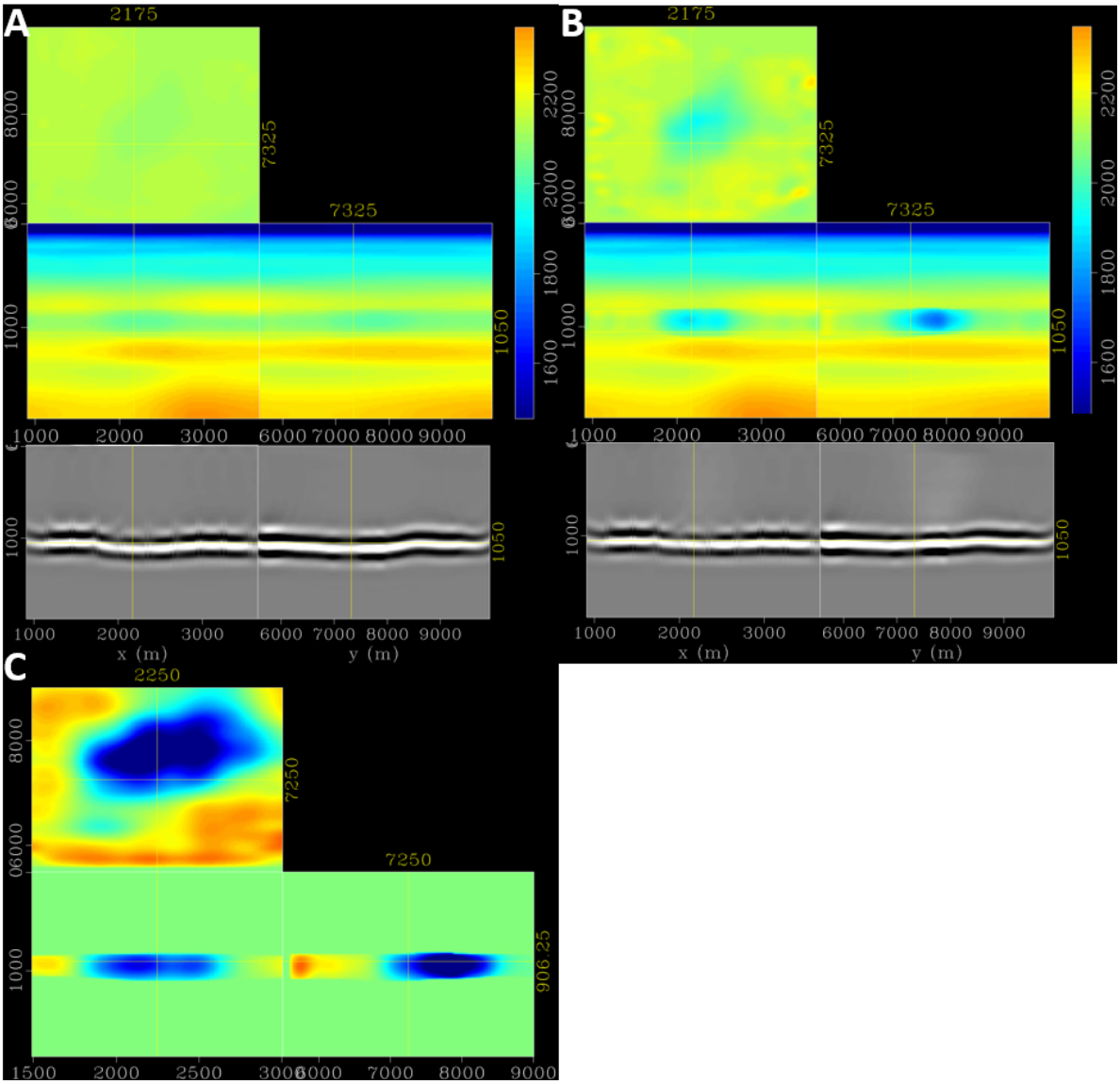

Fig. 4.9: The velocity model for the 2006 monitoring survey, with constraints of the upper and lower boundary of the reservoir (Fig. 4.8a). A and B represents the velocity model after one and two iterations, respectively. The velocity models are used to migrate the Utsira base reflector illustrated below each model. X, Y and Z coordinates are given in meters. C illustrates the difference between the final velocity model and the initial velocity model.

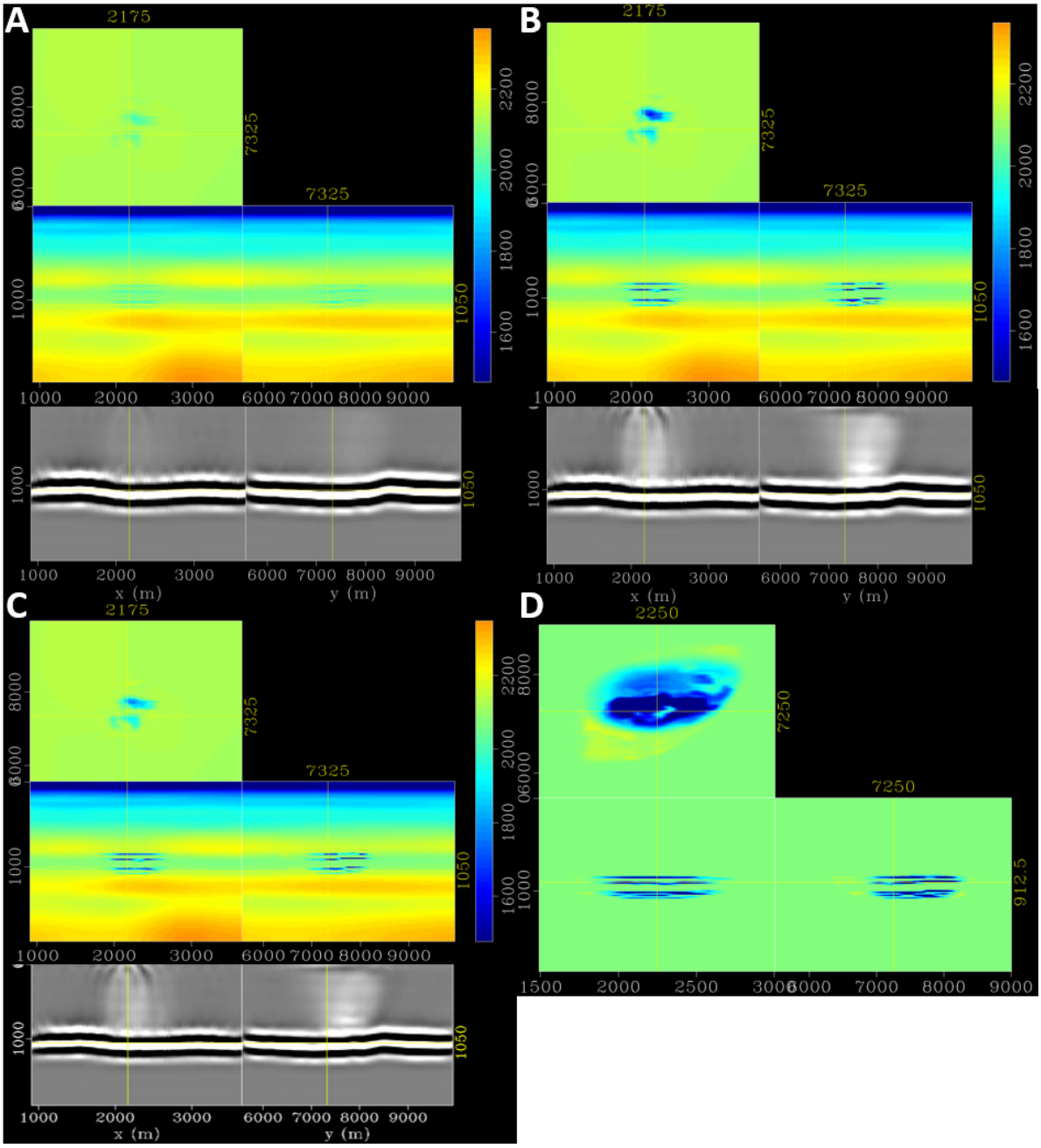

Fig. 4.10: The velocity model for the 2001 monitoring survey, with constraints of the intra-reservoir carbon dioxide accumulations beneath mudstone layers (Fig. 4.8b). A, B and C represents the velocity model after one, two and three iterations, respectively. The velocity models are used to migrate the Utsira base reflector illustrated below each model. X, Y and Z coordinates are given in meters. D illustrates the difference between the final velocity model and the initial velocity model.

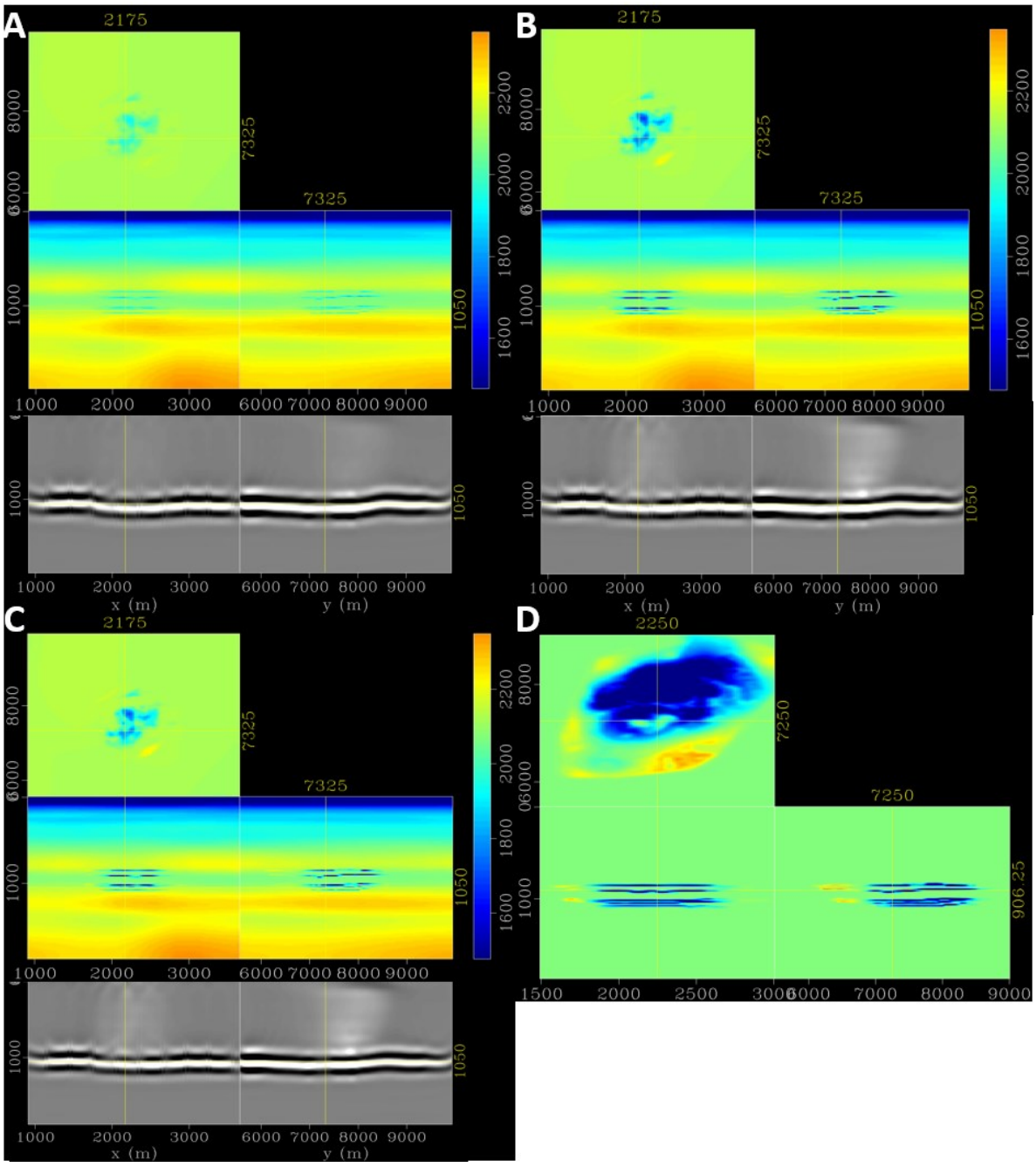

Fig. 4.11: The velocity model for the 2006 monitoring survey, with constraints of the intra-reservoir carbon dioxide accumulations beneath mudstone layers (Fig. 4.8c). A, B and C represents the velocity model after one, two and three iterations, respectively. The velocity models are used to migrate the Utsira base reflector illustrated below each model. X, Y and Z coordinates are given in meters. D illustrates the difference between the final velocity model and the initial velocity model.

When migrating the seismic section with the associated updated velocity model a significant difference in the location of the base reservoir reflector is noticeable. Figure 4.12 and figure 4.13 illustrate how the initial velocity model, the velocity model accounting the whole reservoir as one homogenous package and the model constraining the velocity changes to estimated gas accumulation as a result of intra-reservoir sealing units differently affects the location of the 2001 and 2006 Utsira base reflector, respectively. Compared to the baseline model and the hereby pre-determined locations of key reflectors, all migrated images illustrate an equivalent location of the upper reflector of the reservoir.

However, images generated from both monitor surveys based on the initial velocity model of 1994 illustrates the base reflector with a push-down effect below the gas plume compared to the optimal location of the reflector (Fig. 4.12a; 4.13a). Utilizing the velocity model constraining the reservoir with only the upper and lower boundary of the reservoir, results in a substantial change in the velocity field estimates over the entire reservoir. As the velocity updates are not constrained only to the gas accumulations within the reservoir, the migrated image after updating suffers from a substantial pull-up effect visible at both the lower boundary of the reservoir, in addition to the intra-reservoir reflectors of sealing mudstones (Fig. 4.12b; 4.13b).

When constraining the velocity updates to intra-reservoir sealing units, the velocity changes are determined to take place exclusively in the gas accumulation beneath the sealing units. The intra-reservoir constrained updated velocity model leads to an improved migrated image compared to the one obtained with velocity updates over the whole Utsira formation. This is because it manages to correct for the push-down of the base Utsira reflector without introducing significant artificial pull-up at the reflectors within and beneath the Utsira formation. The updated migrated image also indicates a favorable correlation between the pre-determined location of reflectors and the migrated reflectors (Fig. 4.12c; 4.13c). Both the base boundary of the reservoir and the reflector located directly beneath is migrated to the aiming location, with only small errors in the correlation (Fig. 4.12c; 4.13c).

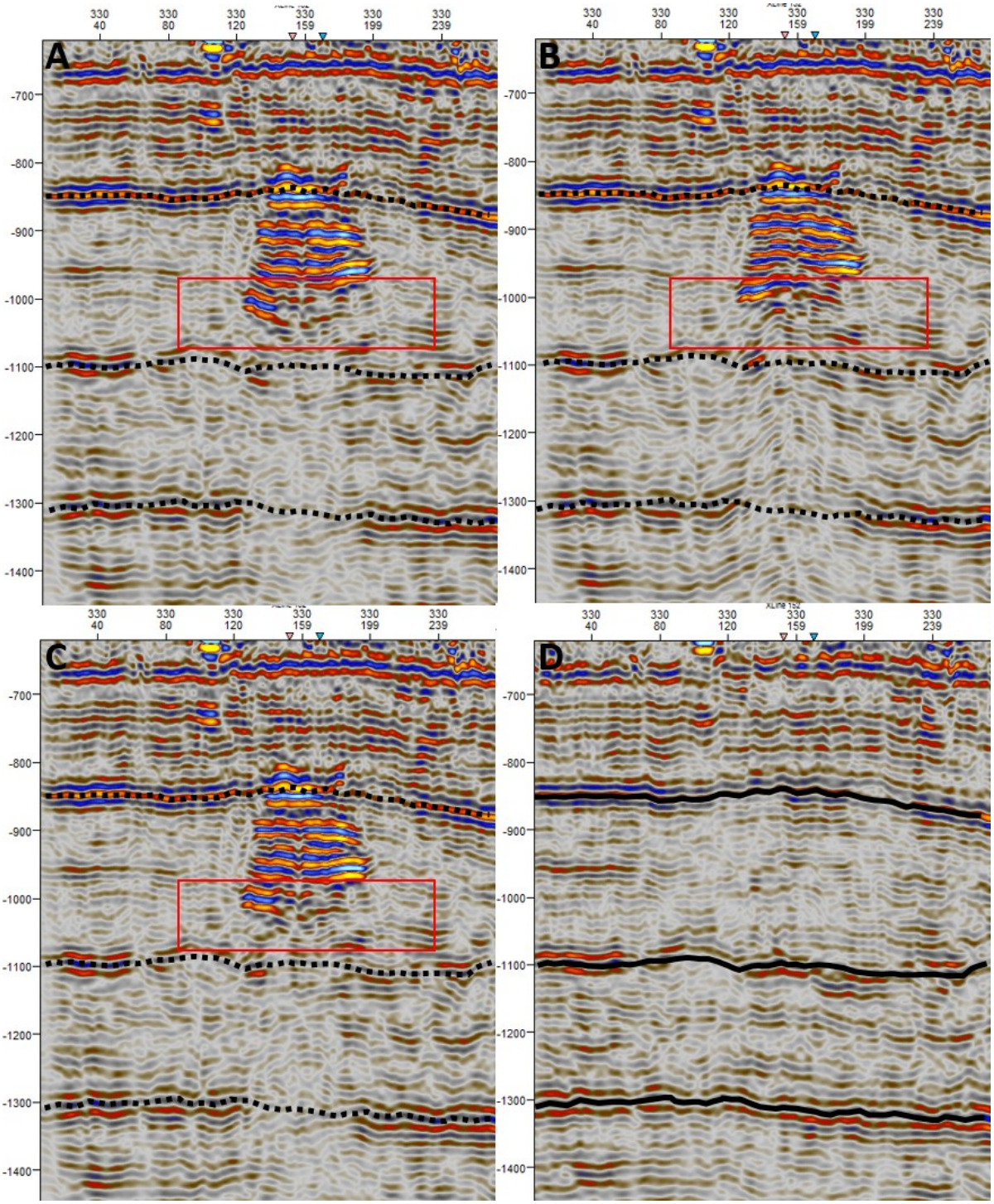

Fig. 4.12: A) Migrated image based on the initial velocity model (1994 dataset). B) Migrated image based on the velocity model constrained by Utsira upper and lower boundary. C) migrated image based on the velocity model constrained by intra-reservoir interpreted reflectors. D) Migrated image of the baseline model. The red square illustrates enhances focusing for reflectors not includes in the velocity model constraints. In addition, the interpreted reflectors on the baseline survey are marked with dashed lines on the monitoring survey to indicate the aiming location of key reflectors.

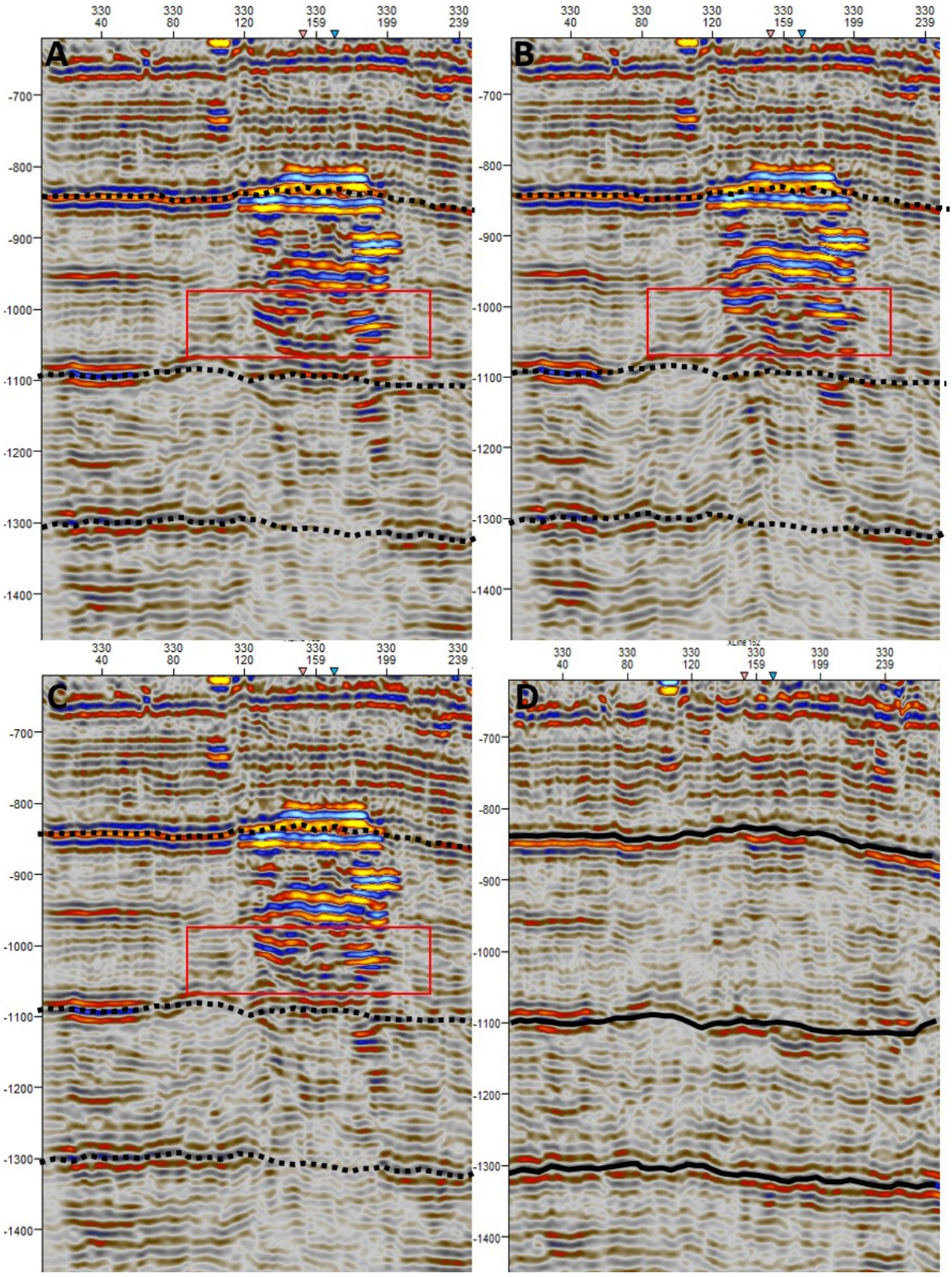

Fig. 4.13: A) Migrated image based on the initial velocity model (1994 dataset). B) Migrated image based on the velocity model constrained by Utsira upper and lower boundary. C) migrated image based on the velocity model constrained by intra-reservoir interpreted reflectors. D) Migrated image of the baseline model. The red square illustrates enhances focusing for reflectors not includes in the velocity model constraints. In addition, the interpreted reflectors on the baseline survey are marked with dashed lines on the monitoring survey to indicate the aiming location of key reflectors.

Chapter 5: Discussion

A continuous monitoring operation at the Sleipner field has confirmed the predicted value of conventional time-lapse seismic surveys for the purpose of monitoring subsurface storage opportunities for carbon dioxide. Prominent amplitude anomalies on the seismic image as a response to the injected CO_2 gives distinct indications of placement of gas accumulations in the reservoir. In addition, such a major effect on the seismic response allows for the assumption that major breakage of the capping rock causing leakage would have been detected. Until this date, leakage has not been observed, indicating a currently safe storage opportunity for superfluous carbon dioxide, reducing the environmental impact of releasing the gas into the atmosphere (Halland et al., 2013).

Time-lapse surveys have contributed with the possibility to observe and predict the movement of the injected gas. The buoyancy effect has allowed the gas to migrate upwards towards the shallowest topographic point of the capping rock structure. However, several intra-reservoir mudstone layers, detected both from the seismic response and from well logs, have created local sealing units within the developed gas plume and has had a significant effect on both the gas distribution and migration pathways from the injection point to the place of accumulation. High porosity and permeability conditions estimated for the reservoir allows for the assumption of straightforward, uncomplicated migration of CO_2 (Chadwick et al., 2004a; Zweigel et al., 2004). Nonetheless, by cause of multiple local storage units supporting and increasing the strength of the overall main capping rock, the reservoir as a whole may have an even higher storage capacity than first estimated.

Close observations of the injection process have given no indication of increasing pressure in the reservoir (Johnston, 2010). Measurements of pressure and temperature conditions in the Utsira Formation from well bores imply that the injected carbon dioxide will remain in a supercritical state as when injected when stored in the subsurface. (Torp & Gale, 2004). The lack of increasing pressure at the wellhead indicates that pressure affecting the seismic velocities is marginal to non-existent.

5.1 Plume development

Topographical maps of the upper and lower boundary of the reservoir have a good correlation to the previously interpreted and previously described depositional environment and direction of the Utsira Formation. Evaluating the thickness distribution of the reservoir by constructing a thickness map from the baseline survey, indicate a depocenter with an NNE-SSW direction and mainly located towards the south of the reservoir is consistent with the assumption of the

main depositional source from the Scandinavian mainland (Fig. 5.1). Mud volcanoes and diapers located at the reservoir base increases the uncertainty in the interpretation of the base reflectors. The migration of this reflector for the baseline survey are considered as the optimal location of the reservoir boundary and hence used as the aiming result for the further analysis of monitoring datasets. Local depth variations have resulted in the interpretation not being straight forward. However, with confirmation from well logs, as well as the correlation of corresponding reflectors in areas with no gas effect, the overall confidence of the reflector location has increased.

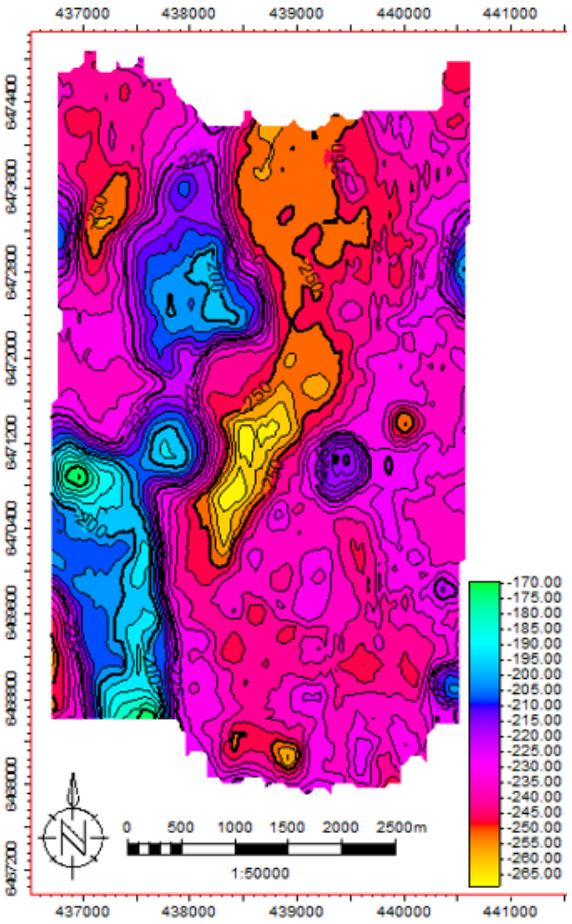

Fig. 5.1: Thickness map constructed from the interpreted upper and lower boundary of the Utsira Formation.

Observations of the interpreted upper boundary of the reservoir indicate a small mismatch in the location even after dataset time-shift is conducted (Fig. 4.2). However, the similarity in topographic structure of the upper boundary compared to the dissimilarity in the structure of the lower boundary gives a good implication of which areas that are affected by velocity decrease due to gas injections.

To fully exploit the reservoir capacity; the carbon dioxide is injected close to the base boundary of the Utsira Formation (Chadwick et al., 2004b). As the reservoir lithology is

consisting of alternating layers of storing sandstone packages and shaly sealing units, the gas has maneuvered upwards as a result of density differences through all flow units (Rafaelsen, 2013). The plume growth is easily determined as a fact due to both vertical and lateral increasing amplitude anomalies in later vintages. As it is not possible to distinguish the mudstone layers located within the reservoir at the baseline survey, the plume development is determined only based on the difference between the two monitor datasets. However, identifiable high amplitudes lacking on the RMS amplitude baseline map, while a detectable growth is seen in the latter vintages, supports the assumption that high amplitude present is caused by carbon dioxide injections (Fig. 4.1).

The distinct vertical migration, mapped out based on the expansion of strong reflectors developed vertically from the injection point to the top of the reservoir in later vintages representing the vertical migration of CO_2, has developed a more than 200 meters high gas column in the reservoir (Fig. 4.1). From the monitoring dataset of 2001, it is already clear that the gas has reached the top seal of the reservoir. The interpretation of monitoring datasets indicates a large chimney structure developed at the center of the reservoir, producing a direct migration route from the injection point to the top seal. As the chaotic signature pattern of the chimney cannot be identified on the baseline survey, several possibilities for the development of the structure can be discussed. One possibility is that the thin sealing mudstone layers have been breached by cause of a developing pressure regime beneath the layers due to constant injection flow of gas. Further, the chimney may be a result of capillary pressure replacing the formation fluids of the sealing units with the injected gas developing a vertical migration route with additional injection. Furthermore, small faults or fractures, below the resolution limit of the seismic image, developed as a result of rapid deposition of the Utsira Formation may have caused the vertical migration (Chadwick et al., 2004b).

Nonetheless, the chimney structure can be interpreted as a result of the presence of gas and the strong energy increase in intra-reservoir negative reflectors suggest a higher amount of CO_2 stored in the center of the reservoir than towards the plume flanks (Fig. 4.1; 4.4). From the interpretation of the Utsira top boundary, the shallowest point is found to be the topographic high located directly above the injection point (Fig. 4.2). The interpretation of center storage of carbon dioxide is strongly confirmed by the pre-injection structure of the reservoir. Due to the difference in density between injected gas and originally in situ brine, the carbon dioxide is expected to migrate towards the capping rocks shallowest location (Chadwick et al., 2008).

In addition, the lateral growth of the reservoir plume is certainly determined as a result of an immense difference in the RMS amplitude maps generated for the reservoir for each monitor dataset. The lateral distribution of the stored CO_2 images an elliptically shaped reservoir, with the long axis orientated in the NNE-SSW direction and the short axis perpendicular (Fig. 4.4). The overall shape is likely to have been developed due to the capping rock topography.

The lateral growth of the long axis is distinctively larger than the short axis, and lateral migration of several hundred meters is observed. RMS amplitude is considered a good direct indicator for the presence of hydrocarbon (Chopra & Marfurt, 2005). As the RMS methodology stack the reflectivity of the subsurface lithology, high impedance contrast due to bed thickness and unit density has an impact on the result. For this reason, hydrocarbon volume calculations made directly from RMS amplitude maps may lead to an overestimation of the reservoir. Nevertheless, the relative development of the gas plume can be determined. The lateral plume development seems to be constrained by the reservoir top and base topography. With a depression surrounded by topographic highs at both the northwestern and southeastern part of the lower reservoir boundary, the gas plume is assumed to have a dominant development in the direction of the plume long axis. Even though a thorough analysis should be made based on several datasets to determine a growth trend, the makeable increase of the long axis in relation to the short axis of the plume gives reason to assume that the short axis will reach its equilibrium before the plume long axis.

5.2 Velocity estimation for the purpose of depth correlation between reflections

The wave-equation migration velocity analysis displays a larger velocity change in the reservoir as a whole and individual layers in the 2006 survey compared to the 2001 survey. As a result of continuous injections, the push-down effect below the reservoir has a significant increase from the 2001 to the 2006 dataset (Fig. 4.1). However, comparing both datasets to the previous ones included in this study, a considerable larger increase in push-down effect is seen between the 2001 and the baseline datasets, than between the 2001 and 2006 dataset. Even when considering the time difference, and hence the difference of injected gas, a non-linear relationship is found. The non-linear relationship is consistent with the previously applied methods such as Gassmann's model for fluid substitution and was therefore expected (Fig. 2.6; Arts et al., 2004a).

Conventional velocity analysis for the purpose of seismic processing includes interval velocity analysis and the traditional Dix equation. Manually picked velocities from common

depth points in the baseline dataset were practiced for the determination of the initial velocity model of this study. The velocity model was utilized in order to create a baseline survey. Due to sharp changes in velocities in the reservoir as a result of carbon dioxide injections, the assumption of a linear perturbation relationship made in the conventional time-shift velocity analysis is violated for monitoring datasets. Hence, when applying this model to the migration process of post-injection seismic data, a severe push-down effect is noticed (Fig. 4.12a; 4.13a). This is a direct result of brine being substituted by carbon dioxide. As gas has a severe effect decreasing the subsurface velocity fields, this expression on the migrated image was expected. Since the resulting velocity decrease in local accumulations of carbon dioxide is not accounted for, it is anticipated that the reflectors beneath the gas accumulation do not match in depth.

Thus, to take into account the strong velocity variation in the Utsira reservoir, the velocity model was iteratively updated using the WEMVA strategy. By performing parallel 3D wave-equation migration velocity analysis on the monitoring dataset, the method results in a more reliable velocity assessment, as opposed to conventional approximate approaches, which commonly restore insufficient velocity estimates and requires post-inversion rescaling. The method operator relates the velocity perturbation to the perturbations of the migrated image and is based on estimating minimum contrast in band-limited waves. Hence, target image fitting performed based on WEMVA naturally handles both multipathing and wave propagation in areas with complex geology.

The WEMVA method intends to obtain and update velocity information from migrated images and aims to develop an image perturbation operator which describes the differences between the monitor image and the baseline model (Yang & Sava, 2011). Wavefield-extrapolation methods, as the WEMVA method, is, unlike ray-based methods, band limited, and will, therefore, contribute to a more precise description of the propagation of waves through areas with complex geology. With the presence of gas cycle skipping problems commonly occurs. Cycle skipping is developed when the location of key reflectors in the migrated images differs by more than half a cycle compared to the baseline location of the corresponding reflector. These challenges are handled by operating with low-frequency data in order to increase the wavelength, as increasing wavelength allows for a larger location discrepancy between the baseline and monitor reflectors and reduces the probability of cycle skipping.

When comparing the resulting migrated images from the first velocity model, constrained by the top and base reflector of the reservoir only, an uplifting effect, known as the pull-up effect, of every reflector below the upper boundary of the Utsira Formation is observed

(Fig. 5.2). Due to an overestimation of the intra-reservoir velocities, false structures are introduced in the depth-migrated image. As a result of constraining the velocity model to a known heterogeneous reservoir comprised of several flow units, with assumptions of a sand package with a homogenous spread of injected gas, spurious pull-ups, with the exception of the constraint boundaries, are introduced. This is an indication that this model of gas saturation is in violation with the seismic data, as it does not correctly allow the positioning of the reflectors, with the exception of the target reflectors, which should be correctly positioned by the target image fitting. This also shows that correct depth positioning of one key reflector is a necessary but not sufficient condition to constrain the positioning of other reflectors underneath. Most of the previous quantitative studies, which are attempting to determine the distribution of the carbon dioxide in the reservoir based on methods such as amplitude intensity and reflection thicknesses, bases their assumptions on models such as the Gassmann's equation which also considers the fluid substitution to be uniform throughout the reservoir. Hence, resulting assumptions and conclusion may contain severe uncertainties.

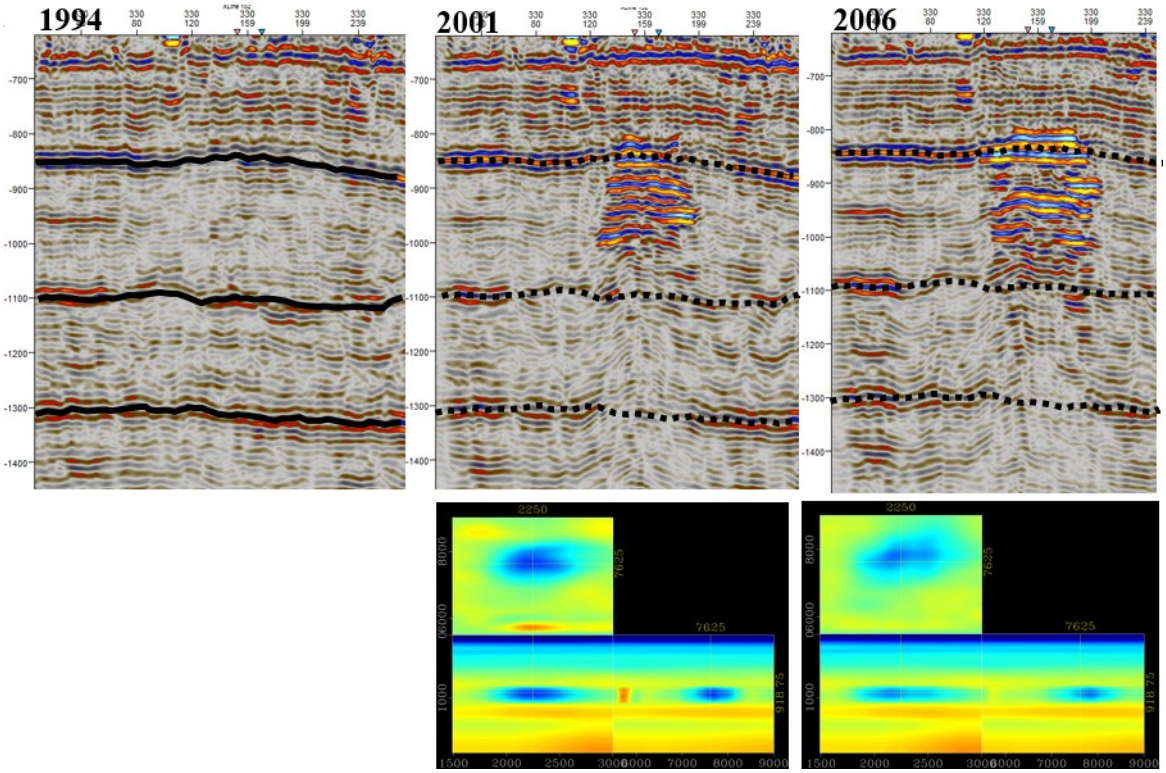

Fig. 5.2: Comparison of a migrated image from the baseline survey and both monitoring surveys, where the migration process is implemented with a velocity model constrained by the top and base reflector of the reservoir only. The interpreted reflectors on the baseline survey are marked with dashed lines on the monitoring surveys to indicate the aiming location of key reflectors.

It is already well known that the reservoir of the Utsira Formation contains shale layers establishing different flow units. As schematically illustrated in figure 5.3, the gas is injected close to the base of the reservoir and accumulates beneath impermeable layers while migrating towards a shallower depth as a result of the buoyancy effect. Even though the signature reflections of the mudstone layers are not visible in the baseline survey, this knowledge must be taken into account. The intensifying reflectors at monitoring surveys expose their location, and the degree of amplitude increase when studying later vintages reveals that the relative amount stored beneath each impermeable layers is increasing over time. Hence, taking this previous knowledge into account, a velocity model with constraints based on local carbon dioxide accumulations within the reservoir is expected to give an adequate result.

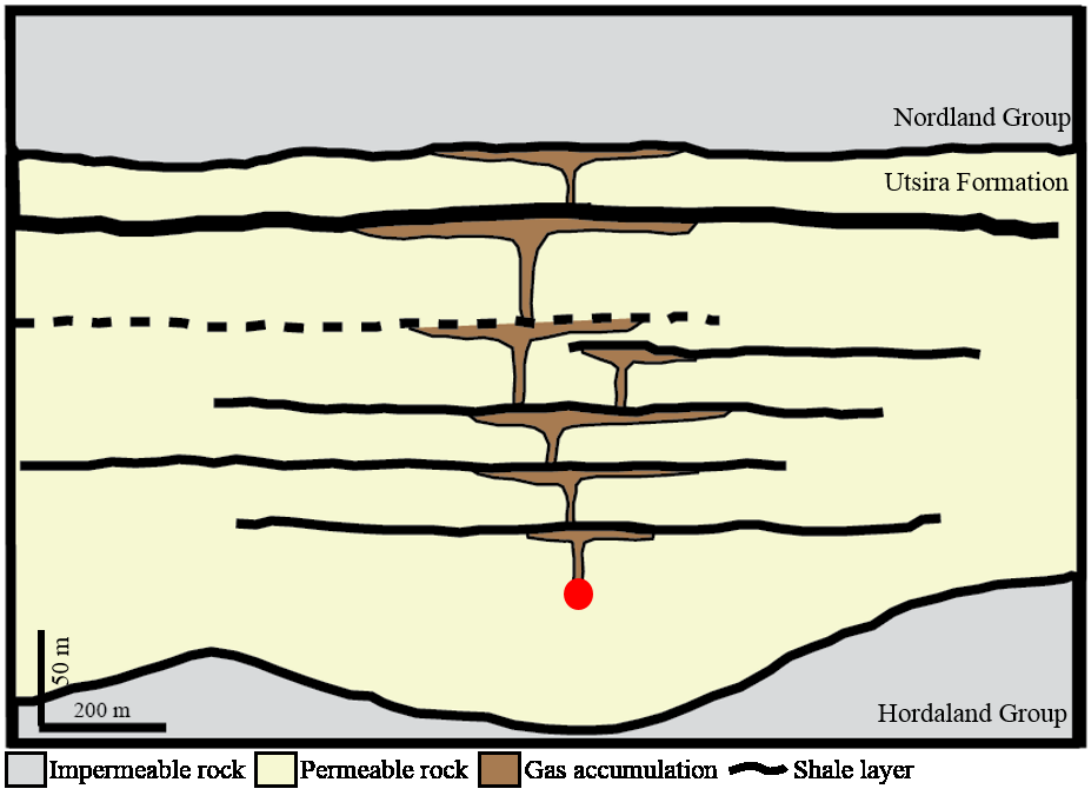

Fig. 5.3: Conceptual illustration of the Utsira reservoir demonstrating the distribution of injected gas. The point of injection is marked with a red disc. The dashed line indicates one of the intra-reservoir shale layers which was not accounted for in this research due to multiple reflectors of the upper boundary of the reservoir.

The aiming objective of the study was to develop a velocity model that would result in depth migrated key reflectors converging to its pre-determined location. The WEMVA method with constraints taking into account the actual framework of the reservoir has a very satisfying result (Fig. 5.4). Both the upper and lower reflector representing the upper and lower boundary of the reservoir is migrated to match its pre-determined location in depth. Additionally, a strong reflector located below the base of the reservoir is tracked and is found to match the location of

the baseline survey. Hence, the WEMVA method has proven to, with proper constraints, serve its purpose of target image fitting.

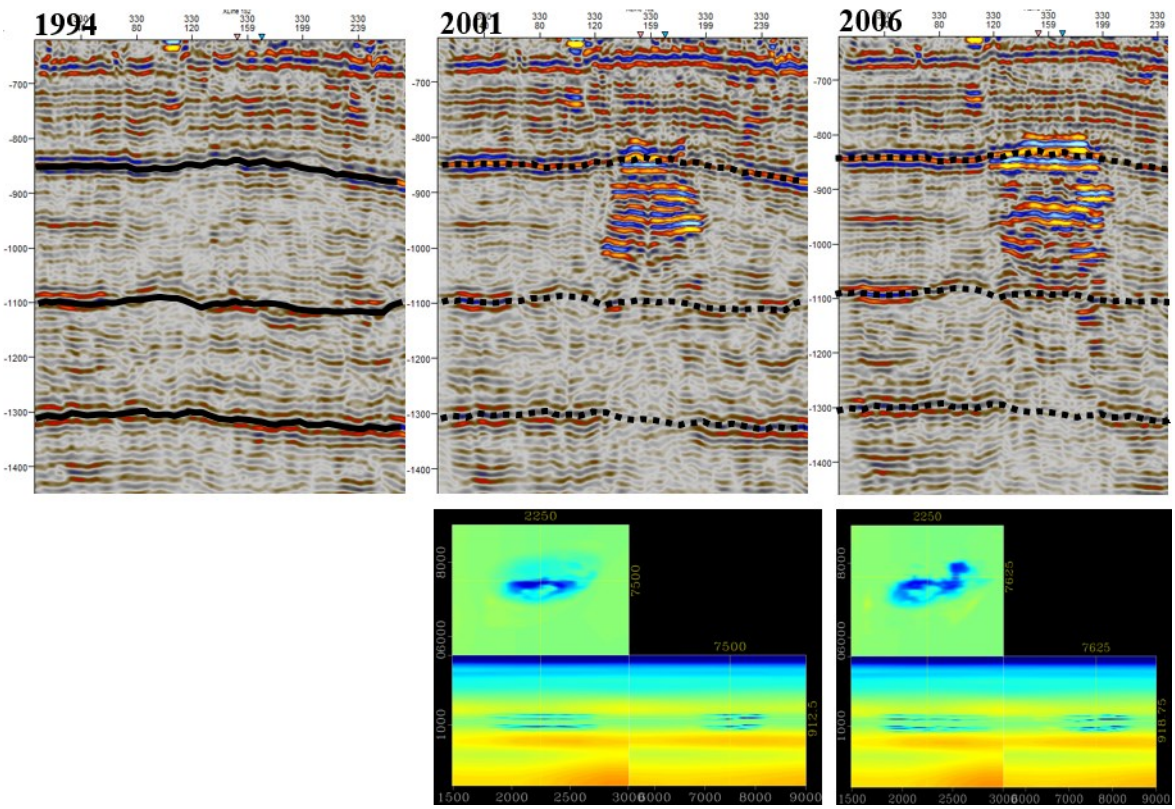

Fig. 5.4: Comparison of a migrated image from the baseline survey and both monitoring surveys, where the migration process is implemented with a velocity model constrained by the interpreted accumulation of carbon dioxide in the reservoir. The interpreted reflectors on the baseline survey are marked with dashed lines on the monitoring surveys to indicate the aiming location of key reflectors.

Despite the satisfying results, it is essential to emphasize the importance of a correctly performed interpretation of key reflectors in each dataset. With a large velocity contrast between gas-saturated and brine-saturated reservoir rock, and chaotic reflection signatures as a result of gas saturation, it is important to take into account that manual interpretation of key reflectors in the time-lapse dataset was not straightforward. In addition, the absence of key reflectors indicating the location of intra-reservoir mudstone layers at the baseline survey, preclude the development of a precise, detailed original reservoir model. With accurate information being absent, uncertainties are to be expected. Further, it must be noticed that a favorable outcome of the WEMVA approach is only fully established if based on accurate and legit prior assumptions.

As the estimate of the image perturbation is complicated, and the time-lapse methodology relies on an accurate estimation of the image perturbation for both the baseline and the monitor dataset, the probability of including uncertainty in the calculated results

increases. Nevertheless, figure 4.12c and 4.13c illustrates how all constraining boundaries are migrated to a more horizontal structure, which was anticipated from previous studies concerning depositional environments for the reservoir (Chadwick et al., 2004a; Halland et al., 2011; Furre & Eiken, 2014). It is shown that with the WEMVA model, which is not only including manually picked travel times but rather are considering the full wavefield, the method achieves a strong velocity model. Hence, using the model when migrating the seismic image, will lead to a more accurate estimation of the reservoir model, and thereby ensure a better description the subsurface structure and its storage opportunity. The results of this study indicate a satisfying convergence of reflectors in the monitoring surveys.

Furthermore, the focusing in the migrated images is also noticed to improve. The shallowest part of the gas plume contains particularly intensified reflectors as a result of gas saturation (Fig. 4.12; 4.13). The enhanced amplitudes naturally increase the focusing of these reflectors. However, when applying the WEMVA strategy, an improved focusing of reflectors located at a deeper depth within the reservoir is also noticed. Despite a chaotic pattern in the seismic section present due to CO_2 saturation and migration, improved focus on intra-reservoir sealing units makes migration routes and chimneys more distinguishable. Consequently, as reflectors located close to the base of the reservoir have an enhanced focusing, a more certain interpretation of their location, as well as extent, is possible to make. The enhanced focusing of the image surrounding the constraints of the WEMVA model indicates that the time-lapse WEMVA method that takes intra-reservoir gas accumulations into account is robust and that the resulting velocity model is a both proper and reliable approaching to the actual subsurface velocity model.

However, to fully achieve correct positioning of subsurface horizons additional information is needed. Wave-equation migration velocity analysis is constrained by the information available in the image-domain using primary reflections. Information normally retrieved from refracted waves and multiples is not attainable. Hence, for further work concerning enhancing the imaging quality in carbon capture and storage projects, it is recommended to integrate the WEMVA method with a method applied to the data-domain, which, at least in theory, takes advantage of all available information of the dataset. An even more robust approach would, therefore, be to apply FWI after an initial estimate of the velocity changes has been made using the WEMVA method. Even though this combination is abnormal, the combination of both methods would reduce the risk of cycle skipping in FWI. Hence, it is possible to utilize the combination by taking advantage of the image-domain WEMVA strategy

to establish an initial model, before applying the full-waveform inversion to reevaluate the previously defined results.

Chapter 6: Conclusion

Utilization of prior knowledge considering underground scattering based on seismic waves has been crucial when imaging the earth's subsurface. With a correctly performed velocity analysis, the seismic images provide necessary information in order to accurately locate key reflectors. Hence, velocity estimation is considered a fundamental procedure when processing reflection seismic data. Accordingly, the described research has developed a more robust approach to determining a velocity model from which the reflectors within the migrated images converges towards its accurate location. The WEMVA strategy focusing on image target fitting proposed in this thesis is based on wavefield-extrapolation in order to address limitations imposed on ray-based velocity models in complex areas with sharp contrast boundaries between velocity fields, which commonly is found in gas saturated reservoirs. By tomographically updating the velocity model to relocate key reflectors to its pre-determined location in depth, the method is used to derive an improved velocity model and enhance image quality for the monitor survey.

From the migrated images applying different velocity models with its unique constraints, the following conclusions can be made:

- Conventional time-shift analysis assuming a linear perturbation relationship has its assumptions violated in CCS projects as a result of sharp velocity changes caused by carbon dioxide injections. Hence, a severe push-down effect on the migrated reflectors is expected when applied in areas containing gas saturation. Furthermore, with previous knowledge of a heterogeneous reservoir, the assumption of a homogenous distribution of carbon dioxide within the reservoir when developing a velocity model results in an overestimation of the intra-reservoir velocities and false structures such as a pull-up effect are introduced on the depth-migrated image.

- Image target fitting using wave-equation migration velocity analysis with constraints to the framework of the heterogeneous reservoir conducted on the monitoring surveys has resulted in migrated images equal to the baseline survey. In addition, enhanced focusing of intra-reservoir reflections not taken into account as constraints in the velocity model is observed. Based on this combination, the velocity model is found to be both robust and solid, and thereby a good approach to the actual subsurface velocity model.

Appendix A: MATLAB-script

```
clear all
close all

%% Load horizons
%% 94
angle=1;
base94=(load('Horizons/Top-bottom/1994_bottom'));
top94=(load('Horizons/Top-bottom/1994_top'));
xb=base94(:,1);
yb=base94(:,2);
zb=base94(:,5);
[xb,yb] = rotatecoords(xb,yb, angle);
xt=top94(:,1);
yt=top94(:,2);
zt=top94(:,5);
[xt,yt] = rotatecoords(xt,yt, angle);


% %% Interpolate horizons to equal grids
[Yq,Xq] = meshgrid(min(yb):12.5:max(yb),min(xb):12.5:max(xb));

F=scatteredInterpolant(xb,yb,zb);
base94q = F(Xq,Yq);
F=scatteredInterpolant(xt,yt,zt);
top94q = F(Xq,Yq);
%

%% 01
base01=(load('Horizons/Top-bottom/2001_bottom'));
top01=(load('Horizons/Top-bottom/2001_top'));
xb=base01(:,1);
yb=base01(:,2);
zb=base01(:,5);
[xb,yb] = rotatecoords(xb,yb, angle);
xt=top01(:,1);
yt=top01(:,2);
zt=top01(:,5);
[xt,yt] = rotatecoords(xt,yt, angle);


% %% Interpolate horizons to equal grids
%[Yq,Xq] =
meshgrid(min(yb):12.5:max(yb),min(xb):12.5:max(xb));
F=scatteredInterpolant(xb,yb,zb);
base01q = F(Xq,Yq);
F=scatteredInterpolant(xt,yt,zt);
top01q = F(Xq,Yq);
%

%% 06
```

```
base06=(load('Horizons/Top-bottom/2006_bottom'));
top06=(load('Horizons/Top-bottom/2006_top'));
xb=base06(:,1);
yb=base06(:,2);
zb=base06(:,5);
[xb,yb] = rotatecoords(xb,yb, angle);

xt=top06(:,1);
yt=top06(:,2);
zt=top06(:,5);
[xt,yt] = rotatecoords(xt,yt, angle);

% %% Interpolate horizons to equal grids
%[Yq,Xq] =
meshgrid(min(yb):12.5:max(yb),min(xb):12.5:max(xb));
F=scatteredInterpolant(xb,yb,zb);
base06q = F(Xq,Yq);
F=scatteredInterpolant(xt,yt,zt);
top06q = F(Xq,Yq);
%


% %% Crop and smooth the surfaces
areax=(50:270);
areay=(150:500);
save grid.mat Xq Yq areax areay;
perc=0.1;
base94q=vel_smoother(base94q(areax,areay), 64, perc, perc, 1);
top94q=vel_smoother(top94q(areax,areay), 64, perc, perc, 1);

base01q=vel_smoother(base01q(areax,areay), 64, perc, perc, 1);
top01q=vel_smoother(top01q(areax,areay), 64, perc, perc, 1);
%
base06q=vel_smoother(base06q(areax,areay), 64, perc, perc, 1);
top06q=vel_smoother(top06q(areax,areay), 64, perc, perc, 1);


%% Plot figures
figure, surf(Xq(areax,areay),Yq(areax,areay),-base94q,
'edgecolor', 'none');
title('Base 94');

figure, surf(Xq(areax,areay),Yq(areax,areay),-top94q,
'edgecolor', 'none');
title('Top 94');



figure, surf(Xq(areax,areay),Yq(areax,areay),-base01q,
'edgecolor', 'none');
title('Base 01');
```

```
figure, surf(Xq(areax,areay),Yq(areax,areay),-top01q,
'edgecolor', 'none');
title('Top 01');

figure, surf(Xq(areax,areay),Yq(areax,areay),-base06q,
'edgecolor', 'none');
title('Base 06');
figure, surf(Xq(areax,areay),Yq(areax,areay),-top06q,
'edgecolor', 'none');
title('Top 06');

% Differences
figure, surf(Xq(areax,areay),Yq(areax,areay),base94q-base01q,
'edgecolor', 'none');
title('Base 94 - Base 01');
figure, surf(Xq(areax,areay),Yq(areax,areay),base94q-base06q,
'edgecolor', 'none');
title('Base 94 - Base 06');
figure, surf(Xq(areax,areay),Yq(areax,areay),base01q-base06q,
'edgecolor', 'none');
title('Base 01 - Base 06');

%% Make reflector models
dt=4;
thickness=3;

Base94 = zeros(601,323,604);
Base01 = zeros(601,323,604);
Base06 = zeros(601,323,604);
for i=1:221
    for j=1:351
        for k=1:601
            t=(k-1)*dt;
            if(t>base94q(i,j) && t < (base94q(i,j)+thickness))
                Base94(k,i+49,j+149) = 1;
            end
            if(t>base01q(i,j) && t < (base01q(i,j)+thickness))
                Base01(k,i+49,j+149) = 1;
            end
            if(t>base06q(i,j) && t < (base06q(i,j)+thickness))
                Base06(k,i+49,j+149) = 1;
            end

        end
    end
end



Fhor=fopen('Base94.bin', 'w');
```

```
fwrite(Fhor, Base94, 'float');
fclose(Fhor);

Fhor=fopen('Base01.bin', 'w');
fwrite(Fhor, Base01, 'float');
fclose(Fhor);

Fhor=fopen('Base06.bin', 'w');
fwrite(Fhor, Base06, 'float');
fclose(Fhor);


%% Load plume horizons
angle=1;
%% 2001_1
plume01_1=(load('Horizons/Within_plume_2001/2001_nr_1'));
xb=plume01_1(:,1);
yb=plume01_1(:,2);
zb=plume01_1(:,5);
[xb,yb] = rotatecoords(xb,yb, angle);


% %% Interpolate horizons to equal grids
load grid;
F=scatteredInterpolant(xb,yb,zb, 'linear', 'none');
plume01_1q = F(Xq,Yq);
figure, h=surf(Xq(areax,areay),Yq(areax,areay),-
plume01_1q(areax,areay), 'edgecolor', 'none');
title('2001 - 1st layer');


%% 2001_2

plume01_2=(load('Horizons/Within_plume_2001/2001_nr_2'));
xb=plume01_2(:,1);
yb=plume01_2(:,2);
zb=plume01_2(:,5);
[xb,yb] = rotatecoords(xb,yb, angle);


% %% Interpolate horizons to equal grids
load grid;
F=scatteredInterpolant(xb,yb,zb, 'linear', 'none');
plume01_2q = F(Xq,Yq);
figure, h=surf(Xq(areax,areay),Yq(areax,areay),-
plume01_2q(areax,areay), 'edgecolor', 'none');
title('2001 - 2nd layer');



%% 2001_4
```

```
plume01_4=(load('Horizons/Within_plume_2001/2001_nr_4'));
xb=plume01_4(:,1);
yb=plume01_4(:,2);
zb=plume01_4(:,5);
[xb,yb] = rotatecoords(xb,yb, angle);


% %% Interpolate horizons to equal grids
load grid;
F=scatteredInterpolant(xb,yb,zb, 'linear', 'none');
plume01_4q = F(Xq,Yq);
%
figure, h=surf(Xq(areax,areay),Yq(areax,areay),-
plume01_4q(areax,areay), 'edgecolor', 'none');
title('2001 - 3rd layer');

%% 2001_5

plume01_5=(load('Horizons/Within_plume_2001/2001_nr_5'));
xb=plume01_5(:,1);
yb=plume01_5(:,2);
zb=plume01_5(:,5);
[xb,yb] = rotatecoords(xb,yb, angle);


% %% Interpolate horizons to equal grids
load grid;
F=scatteredInterpolant(xb,yb,zb, 'linear', 'none');
plume01_5q = F(Xq,Yq);
%
figure, h=surf(Xq(areax,areay),Yq(areax,areay),-
plume01_5q(areax,areay), 'edgecolor', 'none');
title('2001 - 4th layer');


%% 2001_6

plume01_6=(load('Horizons/Within_plume_2001/2001_nr_6'));
xb=plume01_6(:,1);
yb=plume01_6(:,2);
zb=plume01_6(:,5);
[xb,yb] = rotatecoords(xb,yb, angle);


% %% Interpolate horizons to equal grids
load grid;
F=scatteredInterpolant(xb,yb,zb, 'linear', 'none');
plume01_6q = F(Xq,Yq);
%
```

```
figure, h=surf(Xq(areax,areay),Yq(areax,areay),-
plume01_6q(areax,areay), 'edgecolor', 'none');
title('2001 - 5th layer');

%%%%%%%%%%%%%%%%%%%%%%%%%%%%%%%%
%%%%%%%%%%%%%%%%%%%%%%%%%%%%%%%%
%%%%%%%%%%%%%%%%%%%%%%%%%%%%%%%%
%% 2006_1
plume06_1=(load('Horizons/Within_plume_2006/2006_nr_1'));
xb=plume06_1(:,1);
yb=plume06_1(:,2);
zb=plume06_1(:,5);
[xb,yb] = rotatecoords(xb,yb, angle);


% %% Interpolate horizons to equal grids
load grid;
F=scatteredInterpolant(xb,yb,zb, 'linear', 'none');
plume06_1q = F(Xq,Yq);
figure, h=surf(Xq(areax,areay),Yq(areax,areay),-
plume06_1q(areax,areay), 'edgecolor', 'none');
title('2006 - 1st layer');


%% 2006_2

plume06_2=(load('Horizons/Within_plume_2006/2006_nr_2'));
xb=plume06_2(:,1);
yb=plume06_2(:,2);
zb=plume06_2(:,5);
[xb,yb] = rotatecoords(xb,yb, angle);


% %% Interpolate horizons to equal grids
load grid;
F=scatteredInterpolant(xb,yb,zb, 'linear', 'none');
plume06_2q = F(Xq,Yq);
%
figure, h=surf(Xq(areax,areay),Yq(areax,areay),-
plume06_2q(areax,areay), 'edgecolor', 'none');
title('2006 - 2nd layer');



%% 2006_4

plume06_4=(load('Horizons/Within_plume_2006/2006_nr_4'));
xb=plume06_4(:,1);
yb=plume06_4(:,2);
zb=plume06_4(:,5);
[xb,yb] = rotatecoords(xb,yb, angle);
```

```
% %% Interpolate horizons to equal grids
load grid;
F=scatteredInterpolant(xb,yb,zb, 'linear', 'none');
plume06_4q = F(Xq,Yq);
%
figure, h=surf(Xq(areax,areay),Yq(areax,areay),-
plume06_4q(areax,areay), 'edgecolor', 'none');
title('2006 - 3rd layer');

%% 2006_5

plume06_5=(load('Horizons/Within_plume_2006/2006_nr_5'));
xb=plume06_5(:,1);
yb=plume06_5(:,2);
zb=plume06_5(:,5);
[xb,yb] = rotatecoords(xb,yb, angle);


% %% Interpolate horizons to equal grids
load grid;
F=scatteredInterpolant(xb,yb,zb, 'linear', 'none');
plume06_5q = F(Xq,Yq);

%
figure, h=surf(Xq(areax,areay),Yq(areax,areay),-
plume06_5q(areax,areay), 'edgecolor', 'none');
title('2006 - 4th layer');


%% 2006_6

plume06_6=(load('Horizons/Within_plume_2006/2006_nr_6'));
xb=plume06_6(:,1);
yb=plume06_6(:,2);
zb=plume06_6(:,5);
[xb,yb] = rotatecoords(xb,yb, angle);


% %% Interpolate horizons to equal grids
load grid;
F=scatteredInterpolant(xb,yb,zb, 'linear', 'none');
plume06_6q = F(Xq,Yq);
%
figure, h=surf(Xq(areax,areay),Yq(areax,areay),-
plume06_6q(areax,areay), 'edgecolor', 'none');
title('2006 - 5th layer');


%% Make plume models
```

```
dt=4;
thickness=10;

Plumemod01 = zeros(601,323,604);
for i=1:323
    for j=1:604
        for k=1:601
            t=(k-1)*dt;
            if(~isnan(plume01_1q(i,j)))
                if(t>plume01_1q(i,j) && t <
(plume01_1q(i,j)+thickness))
                    Plumemod01(k,i,j) = 1;
                end
            end
            if(~isnan(plume01_2q(i,j)))
                if(t>plume01_2q(i,j) && t <
(plume01_2q(i,j)+thickness))
                    Plumemod01(k,i,j) = 1;
                end
            end
            if(~isnan(plume01_4q(i,j)))
                if(t>plume01_4q(i,j) && t <
(plume01_4q(i,j)+thickness))
                    Plumemod01(k,i,j) = 1;
                end
            end
            if(~isnan(plume01_5q(i,j)))
                if(t>plume01_5q(i,j) && t <
(plume01_5q(i,j)+thickness))
                    Plumemod01(k,i,j) = 1;
                end
            end
            if(~isnan(plume01_6q(i,j)))
                if(t>plume01_6q(i,j) && t <
(plume01_6q(i,j)+thickness))
                    Plumemod01(k,i,j) = 1;
                end
            end
        end
    end
end

Plumemod06 = zeros(601,323,604);
for i=1:323
    for j=1:604
        for k=1:601
            t=(k-1)*dt;
            if(~isnan(plume06_1q(i,j)))
                if(t>plume06_1q(i,j) && t <
(plume06_1q(i,j)+thickness))
                    Plumemod06(k,i,j) = 1;
```

```
                end
            end
            if(~isnan(plume06_2q(i,j)))
                if(t>plume06_2q(i,j) && t <
(plume06_2q(i,j)+thickness))
                    Plumemod06(k,i,j) = 1;
                end
            end
            if(~isnan(plume06_4q(i,j)))
                if(t>plume06_4q(i,j) && t <
(plume06_4q(i,j)+thickness))
                    Plumemod06(k,i,j) = 1;
                end
            end
            if(~isnan(plume06_5q(i,j)))
                if(t>plume06_5q(i,j) && t <
(plume06_5q(i,j)+thickness))
                    Plumemod06(k,i,j) = 1;
                end
            end
            if(~isnan(plume06_6q(i,j)))
                if(t>plume06_6q(i,j) && t <
(plume06_6q(i,j)+thickness))
                    Plumemod06(k,i,j) = 1;
                end
            end
        end
    end
end

save Plume01.mat Plumemod01;
save Plume06.mat Plumemod06;
%%
Fhor=fopen('Plume01.bin', 'w');
fwrite(Fhor, Plumemod01, 'float');
fclose(Fhor);

Fhor=fopen('Plume06.bin', 'w');
fwrite(Fhor, Plumemod06, 'float');
fclose(Fhor);


%% Depth convertion

dz=5;
Nz=401;
dt=4e-3;

load Plume01.mat;
[n1, n2, n3] = size(Plumemod01);
```

```
t=(0:(n1-1))*4e-3;
t=t(1:586);
Plumemod01=Plumemod01(1:586,:,:);
Vels=load('Horizons/Vint.txt');
t1=Vels(:,3)/1000;
v1=Vels(:,4);
vint=interp1(t1,v1,t);
d=zeros(length(vint),1);
for i=1:length(vint)
    d(i) = sum(vint(1:i))*dt/2;
end
%Plume01_depth = zeros(Nz,n2,n3);
z=(0:Nz-1)*dz;
Plume01_depth = interp1(d,Plumemod01,z);
figure, imagesc(z,z,Plume01_depth(:,:,300));



%% Make velocity cube

dx=500;
dy=500;
Nt = 78;
dt = 30;
angle=1;


Vraw = load('../Int_vel_all_4cols.txt');

minx = min(Vraw(:,1));
maxx = max(Vraw(:,1));

miny = min(Vraw(:,2));
maxy = max(Vraw(:,2));

Nx = floor((maxx-minx)/dx) + 1;
Ny = floor((maxy-miny)/dy) + 1;

Vcube = zeros(Nt, Nx, Ny);

for i=1:49608
    x=Vraw(i,1);
    y=Vraw(i,2);
    t=Vraw(i,3);
    v=Vraw(i,4);
    it=t/dt + 1;
    ix=floor((x-minx)/dx)+1;
    iy=floor((y-miny)/dy)+1;
    if(it>Nt)
        it=Nt;
    end
```

```
    if(ix>Nx)
        ix=Nx;
    end
    if(iy>Ny)
        iy=Ny;
    end
    if(it<1)
        it=1;
    end
    if(ix<1)
        ix=1;
    end
    if(iy<1)
        iy=1;
    end
    Vcube(it, ix, iy) = v;
end
Vcube2=Vcube;
for ix=1:Nx
    for iy=1:Ny
        for it=1:Nt
            if(Vcube(it,ix,iy) == 0)
                Vcube2(it,ix,iy) =
mean(mean(Vcube(it,Vcube(it,:) ~= 0)));
            end
        end
    end
end

FVel=fopen('Vint.bin', 'w');
fwrite(FVel, Vcube2);
fclose(FVel);
```

Bibliography

Andreassen, K. (2009). Marine Geophysics, lecture notes for Geo-3123. *University of Tromsø*.

Andrew, J. C., Haszeldine, R. S., & Nazarian, B. (2015). The Sleipner CO_2 storage site: using a basin model to understand reservoir simulations of plume dynamics. *First Break*, *33*(6), 61-68.

Artola, F. A., & Alvarado, V. (2006). Sensitivity analysis of Gassmann's fluid substitution equations: Some implications in feasibility studies of time-lapse seismic reservoir monitoring. *Journal of Applied Geophysics*, *59*(1), 47-62.

Arts, R. (2000). *SACS Internal Report – Note on the seismic data.* Utrecht, the Netherlands: Terrein Unicersity College Utrecht.

Arts, R., Eiken, O., Chadwick, A., Zweigel, P., Van der Meer, L., & Zinszner, B. (2004a). Monitoring of CO_2 injected at Sleipner using time-lapse seismic data. *Energy*, *29*(9), 1383-1392.

Arts, R., Eiken, O., Chadwick, A., Zweigel, P., van der Meer, B., & Kirby, G. (2004b). Seismic monitoring at the Sleipner underground CO_2 storage site (North Sea). *Geological Society, London, Special Publications*, *233*(1), 181-191.

Arts, R. J., Trani, M., Chadwick, R. A., Eiken, O., Dortland, S., & Van Der Meer, L. G. H. (2009). Acoustic and elastic modeling of seismic time-lapse data from the Sleipner CO_2 storage operation. In M. Grobe, J. C. Pashin, & R. I. Dodge (Eds.). *Carbon dioxide sequestration in geological media,* (pp. 391-403). Danvers, Massachusetts: AAPG.

Bickle, M., Chadwick, A., Huppert, H. E., Hallworth, M., & Lyle, S. (2007). Modelling carbon dioxide accumulation at Sleipner: Implications for underground carbon storage. *Earth and Planetary Science Letters*, *255*(1), 164-176.

Boait, F. C., White, N. J., Bickle, M. J., Chadwick, R. A., Neufeld, J. A., & Huppert, H. E. (2012). Spatial and temporal evolution of injected CO2 at the Sleipner Field, North Sea. *Journal of Geophysical Research: Solid Earth*, *117*(B3).

Born, M. (1926). Quantum mechanics of collision processes. *Zeit fur Phys, 38*, 803-827.

Buddensiek, M. L., Sturton, S., & Dillen, M. (2010, June). AVO Analysis of Thin Layers–Application to CO_2 Storage at Sleipner. In *72nd EAGE Conference and Exhibition incorporating SPE EUROPEC 2010*.

Cameron, M., Fomel, S., & Sethian, J. (2008). Time-to-depth conversion and seismic velocity estimation using time-migration velocity. *Geophysics*, *73*(5), VE205-VE210.

Chadwick, A., Arts, R., Bernstone, C., May, F., Thibeau, S., & Zweigel, P. (2008). *Best Practice for the Storage of CO_2 in Saline Aquifers-Observations and Guidelines from the SACS and CO2STORE projects*. Nottingham, UK: British Geological Survey.

Chadwick, R. A., & Noy, D. J. (2010, January). History-matching flow simulations and time-lapse seismic data from the Sleipner CO2 plume. In *Petroleum Geology Conference series* (Vol. 7, pp. 1171-1182). London, UK: Geological Society of London.

Chadwick, R. A., Arts, R., Eiken, O., Kirby, G. A., Lindeberg, E., & Zweigel, P. (2004b). 4D Seismic Imaging of an Injected $C0_2$ Plume at the Sleipner Field, Central North Sea. *Geological Society, London, Memoirs*, *29*(1), 311-320.

Chadwick, R. A., Zweigel, P., Gregersen, U., Kirby, G. A., Holloway, S., & Johannessen, P. N. (2004a). Geological reservoir characterization of a CO_2 storage site: the Utsira Sand, Sleipner, northern North Sea. *Energy*, *29*(9), 1371-1381.

Chadwick, R. A., Arts, R., & Eiken, O. (2005, January). 4D seismic quantification of a growing CO2 plume at Sleipner, North Sea. In *Petroleum Geology Conference series* (Vol. 6, pp. 1385-1399). London, UK: Geological Society of London.

Chadwick, R. A., Noy, D., Arts, R., & Eiken, O. (2009). Latest time-lapse seismic data from Sleipner yield new insights into CO2 plume development. *Energy Procedia*, *1*(1), 2103-2110.

Chadwick, R. A., Williams, G. A., Williams, J. D. O., & Noy, D. J. (2012). Measuring pressure performance of a large saline aquifer during industrial-scale CO 2 injection: The Utsira Sand, Norwegian North Sea. *International Journal of Greenhouse Gas Control*, *10*, 374-388.

Chopra, S., & Marfurt, K. J. (2005). Seismic attributes—A historical perspective. *Geophysics, 70*(5), 3SO-28SO.

Dahlen, F. A., Hung, S. H., & Nolet, G. (2000). Fréchet kernels for finite frequency traveltimes – I. Theory. *Geophysics*, *141*, 157-174.

Delépine, N., Clochard, V., Labat, K., & Ricarte, P. (2011). Post-stack stratigraphic inversion workflow applied to carbon dioxide storage: application to the saline aquifer of Sleipner field. *Geophysical Prospecting*, *59*(1), 132-144.

Eiken, O., Brevik, I., Arts, R., Lindeberg, E., & Fagervik, K. (2000). Seismic monitoring of CO_2 injected into a marine aquifer. *SEG International Exposition and 70th Annual Meeting, Expanded Abstracts,* RC-8.2.

Elliott, S. E., & Wiley, B. F. (1975). Compressional velocities of partially saturated, unconsolidated sands. *Geophysics*, *40*(6), 949-954.

Evans, D., Geological Society of London., Norsk petroleumsforening., & Danmarks og Grønlands geologiske undersøgelse. (2003). *The millennium atlas: Petroleum geology of the central and northern North Sea*. London, UK: The Geological Society of London.

Fornel, A., & Estublier, A. (2013). To a dynamic update of the Sleipner CO_2 storage geological model using 4D seismic data. *Energy Procedia*, *37*, 4902-4909.

Furre, A. K., & Eiken, O. (2014). Dual sensor streamer technology used in Sleipner CO_2 injection monitoring. *Geophysical Prospecting*, *62*(5), 1075-1088.

Færseth, R. B. (1996). Interaction of Permo-Triassic and Jurassic extensional fault-blocks during the development of the northern North Sea. *Journal of the Geological Society*, *153*(6), 931-944.

Galloway, W. E., Garber, J. L., Liu, X., & Sloan, B. J. (1993). Sequence stratigraphic and depositional framework of the Cenozoic fill, Central and Northern North Sea Basin. *Geological Society of London, 4*, 33-43.

Gardner, G. H. F., Gardner, L. W., & Gregory, A. R. (1974). Formation velocity and density—The diagnostic basics for stratigraphic traps. *Geophysics*, *39*(6), 770-780.

Gassmann, F. (1951). Elastic waves through a packing of spheres. *Geophysics*, *16*(4), 673-685.

Ghaderi, A., & Landrø, M. (2009). Estimation of thickness and velocity changes of injected carbon dioxide layers from prestack time-lapse seismic data. *Geophysics*, *74*(2), O17-O28.

Ghazi, S. A. (1992). Cenozoic uplift in the Stord Basin area and its consequences for exploration. *Norsk Geologisk Tidsskrift*, *72*(3), 285-290.

Girard, A., & Vasconcelos, I. (2010). Image-domain time-lapse inversion with extended images. In *SEG Technical Program Expanded Abstracts 2010* (pp. 4200-4204). Society of Exploration Geophysicists.

Gregersen, U., Michelsen, O., & Sørensen, J. C. (1997). Stratigraphy and facies distribution of the Utsira Formation and the Pliocene sequences in the northern North Sea. *Marine and Petroleum geology*, *14*(7-8), 893-914.

Gutierrez, M., Katsuki, D., & Almrabat, A. (2012). Effects of CO_2 injection on the seismic velocity of sandstone saturated with saline water. *International Journal of Geosciences*, *3*(5), 908-917.

Halland, E. K., Johansen, W. T., & Riis, F. (2011). *CO2 Storage Atlas – Norwegian North Sea*. Stavanger, Norway: Norwegian Petroleum Directorate.

Halland, E. K., Bjørnestad, A., Gjeldvik, I.T., Bjørheim, M., Magnus, C., Meling, I.M., Mujezinović J., Riis, F., Rød, R.S, Pham, V.T.H. & Tappel, I. (2013). *CO2 Storage Atlas – Barents Sea*. Stavanger, Norway: Norwegian Petroleum Directorate.

Harrington, J. F., Noy, D. J., Horseman, S. T., Birchall, J. D., & Chadwick, R. A. (2009). Laboratory study of gas and water flow in the Nordland Shale, Sleipner, North Sea. In: M. Grobe, J. C. Pashin, & R. L. Dodge, (Eds.). *Carbon Dioxide Sequestration in Geological Media Ā State of the Science.* (pp. 521-543). Tulsa, Oklahoma: AAPG.

Harvey, L. D. D. (2010). *Carbon-free Energy Supply*. London, UK: Earthscan.

Head, M. J., Riding, J. B., Eidvin, T., & Chadwick, R. A. (2004). Palynological and foraminiferal biostratigraphy of (Upper Pliocene) Nordland Group mudstones at Sleipner, northern North Sea. *Marine and Petroleum Geology*, *21*(3), 277-297.

Holloway, S., Chadwick, R. A., Lindeberg, E., Czernichowski-Lauriol, I., & Arts, R. (2004). *Saline Aquifer CO2 Storage Project (SACS) Best Practice Manual.* Trondheim, Norway: Statoil Research Centre.

IEA Greenhouse Gas R&D Programme (November, 2008). *Aquifer Storage – Development Issues.* IEA GHG.

Isaksen, D., & Tonstad, K. (Eds.). (1989). *A revised Cretaceous and Tertiary lithostratigraphic nomenclature for the Norwegian North Sea*. Stavanger, Norway: Norwegian Petroleum Directorate.

Johnston, D. H. (Ed.). (2010). *Methods and applications in reservoir geophysics*. Huston, Texas: Society of Exploration Geophysicists.

King, M. S. (1966). Wave velocities in rocks as a function of changes in overburden pressure and pore fluid saturants. *Geophysics*, *31*(1), 50-73.

Korbøl, R., & Kaddour, A. (1995). Sleipner vest CO_2 disposal-injection of removed CO_2 into the Utsira formation. *Energy Conversion and Management*, *36*(6), 509-512.

Kumar, D. (2006). A tutorial on Gassmann fluid substitution: formulation, algorithm and Matlab code. *Geohorizons*, *11*, 4-12.

Lothe, A., Emmel, B., Bergmo, P., Mortensen, G. M., & Frykman, P. (2014). *A first estimation of storage potential for selected aquifer cases*. *NORDICCS technical report D25*. Oslo, Norway: SINTEF.

Nanda, N. C. (2016). *Seismic Data Interpretation and Evaluation for Hydrocarbon Exploration and Production*. New York, NY: Springer.

Pham, V. T. H., Riis, F., Gjeldvik, I. T., Halland, E. K., Tappel, I. M., & Aagaard, P. (2013). Assessment of CO_2 injection into the south Utsira-Skade aquifer, the North Sea, Norway. *Energy*, *55*, 529-540.

Pratt, R. G. (1999). Seismic waveform inversion in the frequency domain, Part 1: Theory and verification in a physical scale model. *Geophysics, 64*, 888-901.

Rafaelsen, B. (2013). Petroleum Geology, lecture notes for GEO-3115. *University of Tromsø*.

Raknes, E. B., Weibull, W. W., & Arntsen, B. (2015). Seismic imaging of the carbon dioxide gas cloud at Sleipner using 3D elastic time-lapse full waveform inversion. *International Journal of Greenhouse Gas Control, 42*, 26-45.

Rubino, J. G, & Velis, D. R. (2011). Seismic characterization of thin beds containing patchy carbon dioxide-brine distributions: A study based on numerical simulations. *Geophysics*, *76*(3), R57-R67.

Rundberg, Y. (1991). *Tertiary Sedimentary History and Basin Evolution of the Norwegian North Sea Between 60˚-62˚N: An Integrated Approach*. Trondheim, Norway: Universitetet i Trondheim, Norges tekniske høgskole.

Sava, P. S. (2004*). Migration and Velocity Analysis by Wavefield Extrapolation* (Doctoral dissertation). Stanford, California: Stanford University

Sava, P., & Biondi, B. (2004). Wave-equation migration velocity analysis. I. Theory. *Geophysical Prospecting, 52*(6), 593-606.

Sava, P., Biondi, B., & Etgen, J. (2004). Diffraction-focusing migration velocity analysis with application to seismic and GPR data. *Stanford Exploration* Project, 115, 213-233.

Shragge, J., & Lumley, D. (2013). Time-lapse wave-equation migration velocity analysis. *Geophysics, 78*(2), S69-S79.

Streit, J. E., & Siggins, A. F. (2005). Predicting, monitoring and controlling geomechanical effects of CO2 injection. In *Greenhouse gas control technologies: Proceedings of the 7th International Conference on Greenhouse Gas Control Technologies,* (pp. 643-651). Oxford, UK: Elsevier.

Sturton, S., Buddensiek, M. L., & Dillen, M. (2010, June). AVO analysis of thin layers—application to CO2 storage at Sleipner. In *Proceedings of the 72th. Conference and Exhibition,* (p. 2010). Barcelona, Spain: EAGE.

Torp, T. A., & Gale, J. (2004). Demonstrating storage of CO 2 in geological reservoirs: the Sleipner and SACS projects. *Energy*, *29*(9), 1361-1369.

Valberg, E. (2014). *Time-lapse seismic interpretation of injected CO_2 plume at the Sleipner Field, North Sea* (Master's thesis). Tromsø, Norway: The Arctic University of Norway.

Velis, D. R., & Rubino, J. G. (2011). Quantitative characterization of CO2-bearing thin layers at the Sleipner field using spectral inversion. In: *SEG Technical Program Expanded Abstracts 2011,* (pp. 2502-2506). Tulsa, Oklahoma: Society of Exploration Geophysicists.

Williams, G., & Chadwick, A. (2012). Quantitative seismic analysis of a thin layer of CO_2 in the Sleipner injection plume. *Geophysics*, *77*(6), R245-R256.

Wyllie, M. R. J., Gregory, A. R., & Gardner, L. W. (1956). Elastic wave velocities in heterogeneous and porous media. *Geophysics*, *21*(1), 41-70.

Yang, T., & Sava, P. (2010). Wave-equation migration velocity analysis with extended common-image-point gathers. In: *SEG Technical Program Expanded Abstracts 2010* (pp. 4369-4374). Tulsa, Oklahoma: Society of Exploration Geophysicists.

Yang, T., & Sava, P. (2011). Wave-equation migration velocity analysis with time-shift imaging. *Geophysical Prospecting, 59*(4), 1365-2478.

Zweigel, P., Arts, R., Lothe, A. E., & Lindeberg, E. B. (2004). Reservoir geology of the Utsira Formation at the first industrial-scale underground CO2 storage site (Sleipner area, North Sea). *Geological Society, London, Special Publications*, *233*(1), 165-180.